Article

Cell

# Competitive Disinhibition Mediates Behavioral Choice and Sequences in *Drosophila*

## Graphical Abstract

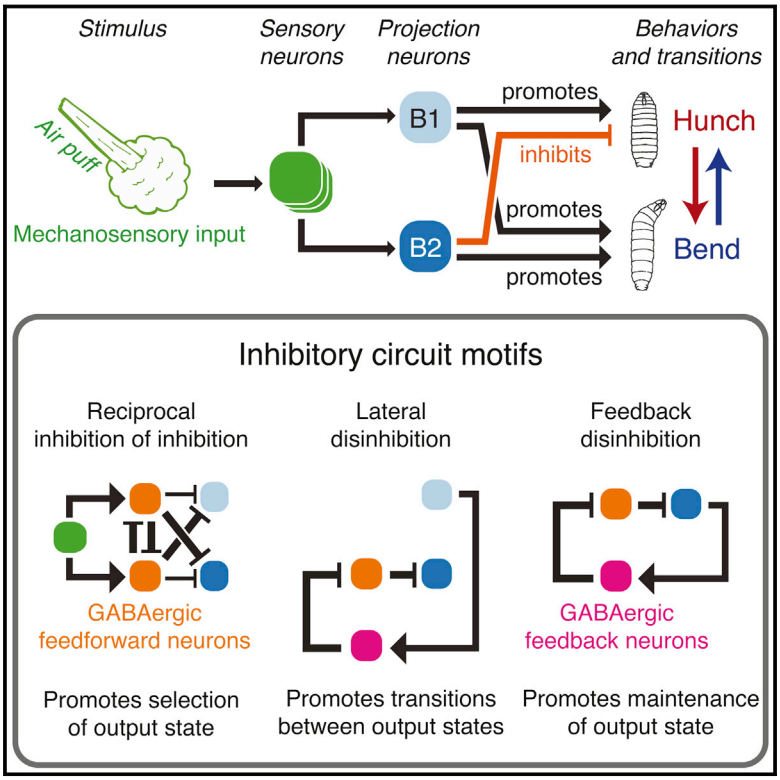


## Highlights

- Mechanical stimuli in *Drosophila* larvae evoke hunch, bend, or a sequence of the two
- Reciprocally connected feedforward inhibitory interneurons mediate behavioral choice
- Feedback disinhibition of projection neurons biases and stabilizes behavioral choice
- Lateral disinhibition of projection neurons promotes sequence transitions

## Authors

Tihana Jovanic, Casey Martin Schneider-Mizell, Mei Shao, ..., James William Truman, Albert Cardona, Marta Zlatic

## Correspondence

schneidermizellc@hhmi.org (C.M.S.-M.), cardonaa@hhmi.org (A.C.), zlaticm@hhmi.org (M.Z.)

## In Brief

Neural circuitries for behavioral choice and sequence are revealed by integrating optogenetic manipulation, electrophysiology, modeling, and EM reconstruction of neuronal networks.

Jovanic et al., 2016, Cell *167*, 1–13
October 20, 2016 
http://dx.doi.org/10.1016/j.cell.2016.09.009

CellPress

Please cite this article in press as: Jovanic et al., Competitive Disinhibition Mediates Behavioral Choice and Sequences in *Drosophila*, Cell (2016), http://dx.doi.org/10.1016/j.cell.2016.09.009

Article

Cell

# Competitive Disinhibition Mediates Behavioral Choice and Sequences in *Drosophila*

Tihana Jovanic,[1,4] Casey Martin Schneider-Mizell,[1,4,*] Mei Shao,[1] Jean-Baptiste Masson,[1,2,3] Gennady Denisov,[1] Richard David Fetter,[1] Brett Daren Mensh,[1] James William Truman,[1] Albert Cardona,[1,*] and Marta Zlatic[1,5,*]

[1]Janelia Research Campus, Howard Hughes Medical Institute, 19700 Helix Drive, Ashburn, VA 20147, USA

[2]Physics of Biological Systems, Pasteur Institute, 75015 Paris, France

[3]Centre National de la Recherche Scientifique, UMR 3525, 75016 Paris, France

[4]Co-first author

[5]Lead contact

*Correspondence: schneidermizellc@hhmi.org (C.M.S.-M.), cardonaa@hhmi.org (A.C.), zlaticm@hhmi.org (M.Z.)

http://dx.doi.org/10.1016/j.cell.2016.09.009

## SUMMARY

**Even a simple sensory stimulus can elicit distinct innate behaviors and sequences. During sensorimotor decisions, competitive interactions among neurons that promote distinct behaviors must ensure the selection and maintenance of one behavior, while suppressing others. The circuit implementation of these competitive interactions is still an open question. By combining comprehensive electron microscopy reconstruction of inhibitory interneuron networks, modeling, electrophysiology, and behavioral studies, we determined the circuit mechanisms that contribute to the *Drosophila* larval sensorimotor decision to startle, explore, or perform a sequence of the two in response to a mechanosensory stimulus. Together, these studies reveal that, early in sensory processing, (1) reciprocally connected feedforward inhibitory interneurons implement behavioral choice, (2) local feedback disinhibition provides positive feedback that consolidates and maintains the chosen behavior, and (3) lateral disinhibition promotes sequence transitions. The combination of these interconnected circuit motifs can implement both behavior selection and the serial organization of behaviors into a sequence.**

## INTRODUCTION

Animals can respond to a stimulus with a single coordinated action or a sequence of actions. Presentation of a given stimulus at different times can result in a variety of innate responses, both across and within individuals (Barker and Baier, 2015; Gordus et al., 2015; Ohyama et al., 2015; Vogelstein et al., 2014). The selection of one of the possible innate responses at any given time constitutes an elementary form of sensorimotor decision-making. Many perceptual or behavioral states are mutually exclusive (e.g., by virtue of body mechanics), so neural modules mediating different behavioral states are thought to suppress each other. Such competitive interactions may underlie the winner-take-all aspect of behavioral choice and may also serve to stabilize the chosen behavior by preventing transitions. However, mechanisms must also exist to promote transitions between behaviors to enable sequences of actions.

The competitive interactions among functionally distinct neural modules likely involve inhibitory synaptic mechanisms. Evidence for this is found in several phyla and brain areas (Baca et al., 2008; Cui et al., 2013; Goddard et al., 2014; Hikosaka et al., 2000; Kovac and Davis, 1977; Mink, 1996; Mysore and Knudsen, 2012; Sridharan and Knudsen, 2015). Specific circuit architectures have been proposed that could implement selection through competitive interactions; such as reciprocal inhibition between nodes promoting different choices, or lateral inhibition coupled with recurrent excitation between nodes promoting the same choice (Redgrave et al., 2011; Sridharan and Knudsen, 2015; Wang, 2008).

Probabilistic behavioral sequences, such as human typing or fly grooming are also well described by similar classes of models proposing that all actions in a sequence are activated in parallel and the order is established through a hierarchy of reciprocal inhibitory interactions (Bullock, 2004; Kristan, 2014; Lasley, 1951; Seeds et al., 2014). However, identifying the detailed architecture of inhibitory networks corresponding to the implementation of such models, in a specific nervous system with synaptic resolution, has been difficult. This is mainly due to the challenges of determining which defined inhibitory interneuron types are causally related to competing behaviors and in determining the connectivity between neurons that promote distinct behaviors. Even in higher invertebrate nervous systems, where activity of uniquely identifiable neurons can be correlated with specific behavioral choices (Briggman and Kristan, 2006; Briggman et al., 2005; Kristan, 2008; von Reyn et al., 2014), in most cases synaptic-resolution wiring diagrams between neurons involved are unknown.

Here, we investigated the circuit mechanism of behavioral choice and sequence generation in *Drosophila* larvae, in response to a gentle mechanical stimulus. In this system we could use electron microscopy (EM) reconstruction to detail the architecture of inhibitory networks involved in a behavioral choice and determine the roles of individual cell types using intracellular recordings and targeted manipulation of neural activity.

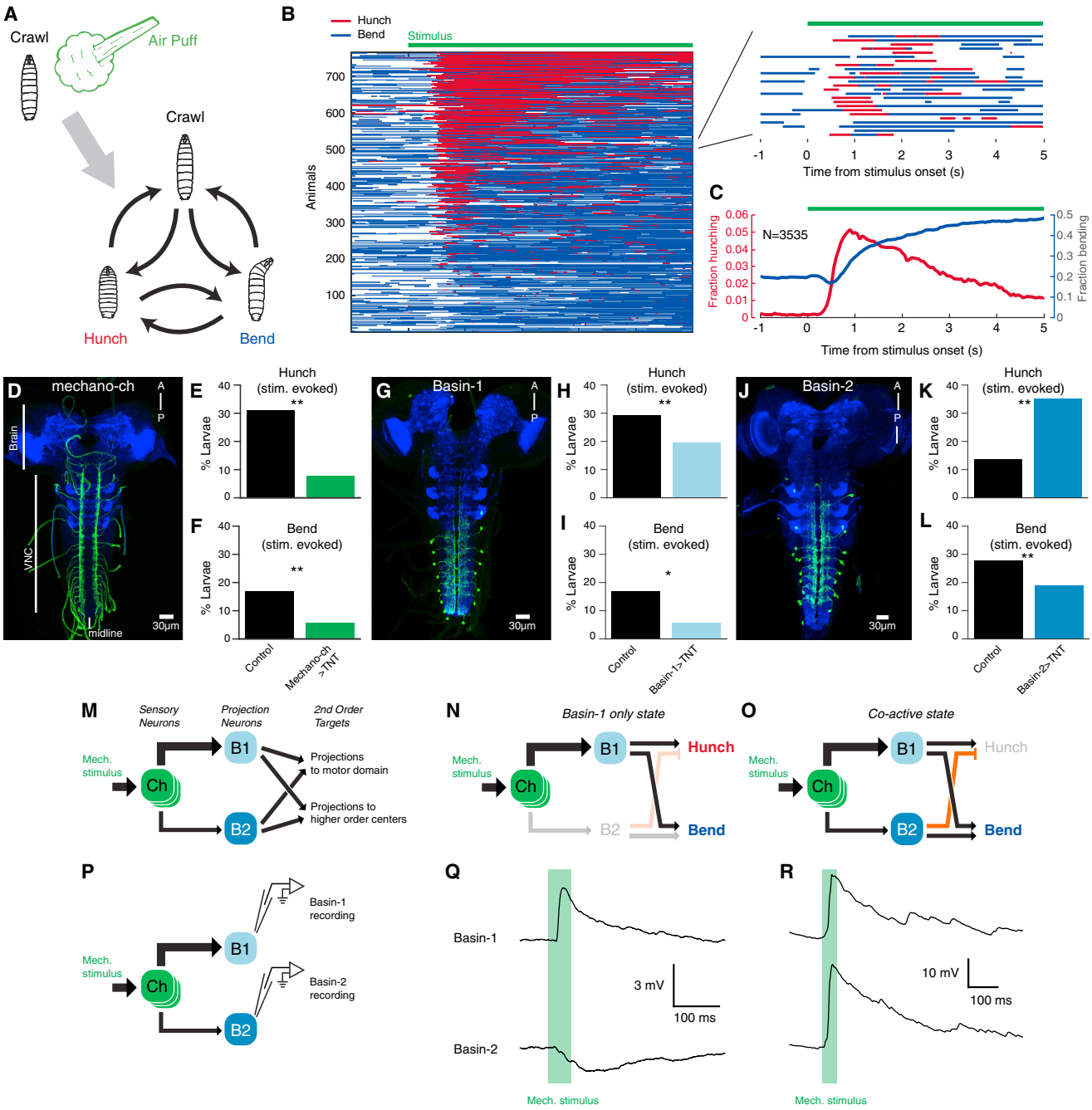


**Figure 1. Different Actions Require Different Combinations of Somatosensory Projection Neurons**

(A) In response to air-puff larvae perform a probabilistic sequence of hunching, bending, and returning to crawling.

(B) Left, ethogram of wild-type larval reaction to air-puff (green line) based on automated behavioral detection. Each row is a larva, hunching (red) or bending (blue). Only those animals with any hunching behaviors after stimulus onset are shown for clarity. Top right, zoom of several individuals. Air-puff speed is 6 m/s.

(C) Fraction of all larvae performing hunch or bend behaviors during stimulus onset.

(D) Dorsal projection of a confocal stack of *R61D08* driving expression of GFP (green) specifically in mechano-ch neurons. Blue, N-cadherin staining to indicate neuropil.

(E and F) Percentage of animals performing stimulus-evoked hunching (E) and bending (F) in response to an air-puff for control larvae (black) and larvae with mechano-ch neurons silenced by targeted expression of TNT (green).

(G) Dorsal projection of a confocal stack of *R20B01* driving expression of GFP specifically in Basin-1 neurons. Colors and labels as in (D).

(H and I) Percentage of animals performing stimulus-evoked hunching (H) and bending (I) in response to air-puff for control larvae (black) and larvae with Basin-1 neurons silenced by targeted expression of TNT (light blue).

*(legend continued on next page)*

## RESULTS

### Mechanosensory Stimuli Stochastically Evoke Different Actions and Action Sequences

We used a high-throughput assay to measure larval behavioral responses to a gentle mechanical stimulus (Ohyama et al., 2013). We found that in response to an air-puff larvae chose to explore the environment by turning their head (a "bend") (Gomez-Marin et al., 2011; Lahiri et al., 2011), or to protect their head by retracting it (a startle-response, we call a "hunch") (Kernan et al., 1994; Ohyama et al., 2013; Tsubouchi et al., 2012), or to perform a probabilistic sequence of the two (Figures 1A–1C, S1A–S1E, and S1H–S1J). Both bend and hunch are discrete motor actions that are readily detectable with automated algorithms (Figure S1A) (Lahiri et al., 2011; Ohyama et al., 2013).

Even repeated presentation of the same stimulus to the same animal evoked bending on some trials and hunching on others (Figures S1D and S1E). We confirmed that the mechanosensory chordotonal (mechano-ch) neurons were involved in triggering both actions (Ohyama et al., 2013; Zhang et al., 2013) (Figures 1D–1F). To exclude the possibility that differences in mechanical stimulus (due to turbulence) were causing the differences in responses, we optogenetically activated the mechano-ch neurons with an identical light stimulus. Repeated activation of the same neurons in the same animal sometimes evoked bending and sometimes hunching (Figures S1F and S1G).

### Different Actions Require Different Combinations of Somatosensory Projection Neurons

To identify the circuit mechanisms implementing this sensorimotor decision we looked for neurons whose activity is differentially required for triggering the two actions (Figures 1G–1M). We started by looking at the neurons immediately downstream of mechano-ch sensory neurons because sensorimotor decisions could happen anywhere along sensorimotor pathways (Barker and Baier, 2015; Cisek, 2007; Gaudry and Kristan, 2009; von Reyn et al., 2014). We had previously identified the Basin projection neurons (PNs), Basin-1, -2, -3, and -4, that receive different combinations of mechanosensory (and nociceptive) inputs and showed that they are excitatory (Ohyama et al., 2015). Downstream targets of Basins project both to the motor domain and to higher order centers such as the brain, suggesting they can act as a hub to convey information to both local and global motor programs (Ohyama et al., 2015) (Figure 1M). Basins were previously implicated in multisensory integration and in promoting the most vigorous rolling escape behavior in response to combined mechanosensory and noxious cues (Ohyama et al., 2015).

To test their role in hunching and bending in response to a mechanical cue alone, we selectively inhibited synaptic transmission (see the STAR Methods) in specific Basin PNs (Figures 1D–1J). Selective inactivation of Basin-1 reduced the likelihood of stimulus-evoked hunching and bending (Figures 1G–1I). In contrast, selective inactivation of Basin-2 (Figures 1I–1L) or Basin-4 (Figure S2A) increased the likelihood of stimulus-evoked hunching and decreased the likelihood of stimulus-evoked bending. These inactivation phenotypes suggest, first, that hunch is promoted when Basin-1 is active alone (Basin-1-only state) and Basin-2 (or Basin-4 or both) is inactive (Figure 1N), and second, that bend is promoted when Basin-1 is co-active with Basin-2 (or Basin-4 or both) (Figure 1O).

Consistent with this idea we found that optogenetic activation (see the STAR Methods) of Basin-1 alone promotes hunching and bending (Figure S2C), whereas optogenetic co-activation of Basins (or of Basin-2 alone) promotes bending, but suppresses hunching (Figures S2D and S2E).

### Mechanosensory Stimuli Stochastically Activate Different Combinations of Somatosensory Projection Neurons

To confirm that mechanosensory stimuli can evoke two distinct Basin activity states, we performed double-patch-clamp intracellular recordings from Basin-1 and Basin-2 in semi-dissected preparations (Figures 1P and S3A–S3C). We observed the predicted Basin-1-only (Figure 1Q) and the co-active states (Figure 1R). The responses of Basin neurons to mechanical stimuli were highly variable both between individuals (Figures 1Q, 1R, and S3C) and between trials within an individual (Figure S3C). The relative frequencies of the two activity states were similar to the relative hunch and bend frequencies in freely behaving

(J) Dorsal projection of a confocal stack of split-Gal4 line *JRC-SS00739* driving GFP in Basin-2 neurons. Colors and labels as in (D).

(K and L) Percentage of animals performing stimulus-evoked hunching (K) and bending (L) in response to air-puff for control larvae (black) and larvae with Basin-2 neurons silenced by targeted expression of TNT (dark blue).

(M) Established synaptic connectivity of mechano-ch neurons and Basin cells (Ohyama et al., 2015)

(N) A proposed Basin-1 only active state promotes both hunch and bend behaviors.

(O) A proposed Basin-1 and Basin-2 co-active state promotes bend behaviors and suppresses hunch.

(P) Schematic of double-patch recordings from Basin-1 and Basin-2 in response to a mechanical stimulus.

(Q and R) Example recordings from Basin-1 and Basin-2 in two different individuals in response to a mechanical stimulus. In a semi-dissected preparation, a mechanical stimulus (piezo, 1,000 Hz, 50 ms) evokes either a Basin-1 only state or a co-active state. No Basin-2 on, Basin-1 off state was observed across in 145 trials across 16 animals.

For behavioral experiments, stimulus-evoked responses were calculated as the difference in fraction of animals performing a behavior post-stimulus and pre-stimulus. Control animals have the GAL4 driving an inactive form of TNT (impTNT). Computation of p value for a difference between stimulus-evoked responses was performed using numerical simulation (see Quantification and statistical analysis in the STAR Methods). Test larvae are *R61D08 > UAS-TNT* (mechano-ch), *R20B01 > UAS-TNT* (Basin-1), and *JRC-SS00739 > UAS-TNT* (Basin-2). Control is a GAL4 control (in black): GAL4 > UAS-impTNT (inactive TNT): R61D08 > UAS-impTNT (mechano-ch), *R20B01 > UAS-impTNT* (Basin-1), and *JRC-SS00739 > UAS-impTNT*, respectively. The number of larvae and exact p values for all the experiments in all figures are specified in Table S1. *$p < 0.05$, **$p < 0.001$ in all figures.

See also Figures S1, S2, and S3 and Tables S1 and S3.

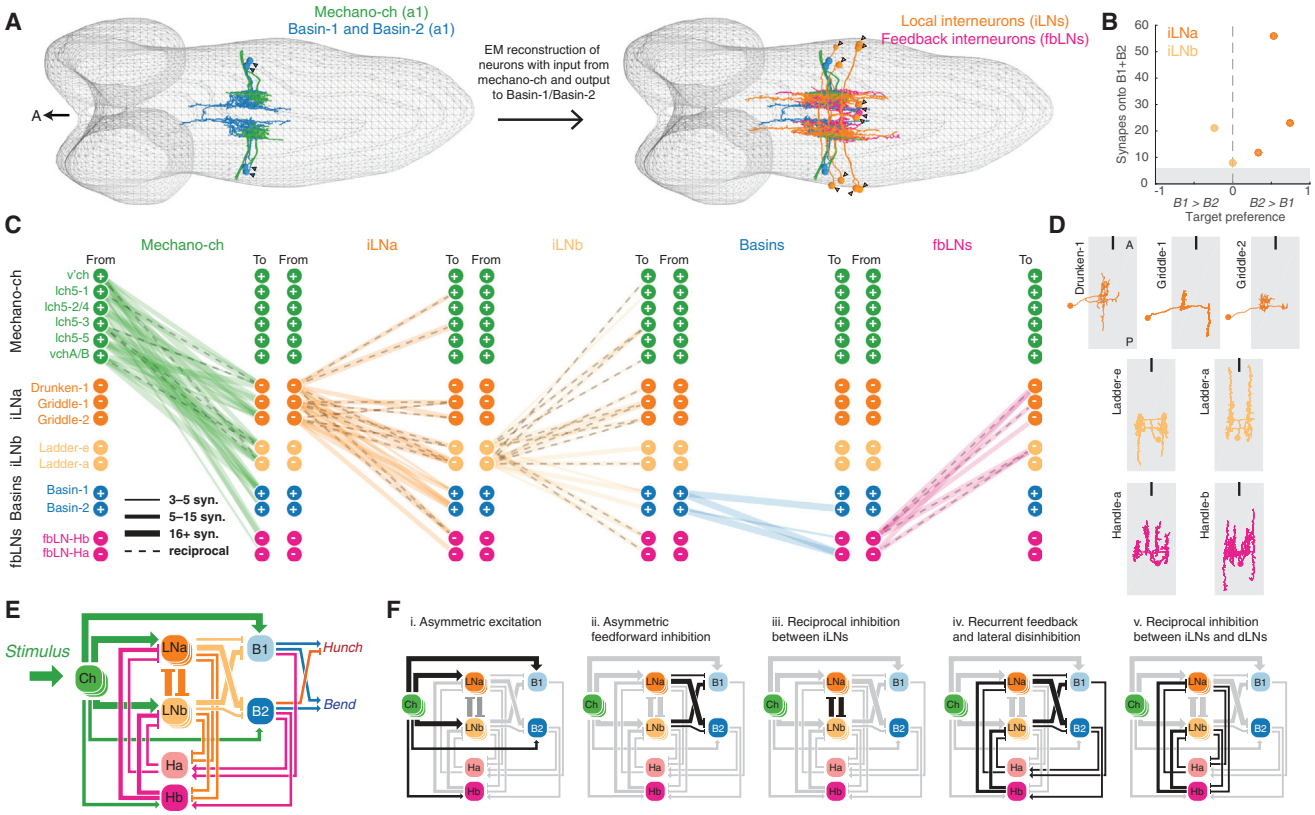


**Figure 2. EM Connectome Reveals a Complex Network of Interconnected Interneurons Innervating Somatosensory PNs**

(A) Dorsal view of EM reconstructions of Basin and mechano-ch cells in abdominal segment a1 (left, data from Ohyama et al., 2015) and all neurons synaptically downstream of mechano-ch and upstream of Basin cells (orange) or feedback local interneurons (magenta). Arrowheads indicate cell bodies.

(B) Interneuron synaptic preference for Basin-1 versus Basin-2 (measured as the difference between synapses onto the two types normalized by the sum) versus total number of synapses made onto either Basin. Five LN types make strong connections ($\geq$5 synapses) onto Basin-1 and Basin-2. Three preferred Basin-2 (collectively, iLNa), while one preferred Basin-1 and one was exactly balanced (collectively, iLNb).

(C) Wiring diagram of the Basin circuit. Each row is a cell type; lines indicate a $\geq$3 synapse connection from left onto right. For consistency, we only show connections found in two or more hemisegments. Each column shows only connections postsynaptic to one neuronal category. Number of synapses is indicated by edge width (see legend). Reciprocated edges are highlighted with a dashed line. Nodes marked with (+) indicate excitatory neurons, those with (–) are GABAergic (Figures S4D–S4S).

(D) Dorsal views of interneurons as reconstructed from EM. Grey box indicates neuropil, black dash the midline. Neuropil box is 40-μm wide.

(E) Schematic of the reconstructed Basin circuit. Edge width increases with number of synapses. Sharp arrowheads are excitatory, squared inhibitory.

(F) Motifs in the observed wiring diagram that could contribute to determining network output state.

See also Figures S4 and S5 and Data S1 and S2.

animals (Figures S1D, S1E, S1H–S1J, and S3C), providing further support for the model that hunch is promoted when Basin-1 is active alone (Basin-1-only state) and that bend is promoted when Basin-1 is co-active with Basin-2 (Figure 1O).

## EM Connectome Reveals Different Inhibitory Interneuronal Types Innervating the Projection Neurons

Next, we asked if inhibition could shape Basin responses. Using patch-clamp recording from Basin-1 in response to a mechanosensory stimulus before and after application of GABA-A receptor antagonist (picrotoxin) we confirmed that these neurons were subject to inhibition (Figures S4A–S4C).

To identify the specific inhibitory neurons responsible, we performed comprehensive EM reconstruction (Schneider-Mizell et al., 2016) of local neurons (LNs) synaptically upstream of Basin PNs and downstream of mechano-ch terminals (Figures 2A–2D and S5A–S5D; Data S1 and S2) in an EM volume spanning the entire larval CNS (Ohyama et al., 2015). We identified four distinct hemilineages (families) of LNs, with multiple neurons per family (Figure 2D). We used lines that drove gene expression (selectively or non-selectively) in at least one member of each family to target GFP to the LNs and co-stained with an antibody against GABA (Li et al., 2014; Pfeiffer et al., 2010). All three families were GABA-positive and hence likely inhibitory LNs (Figures S4D–S4S).

We categorized LNs based on their connectivity with Basins into those that made numerically strong connections (at least five synapses) onto Basins (feedforward iLNs), those that received inputs from Basins (feedback, fbLNs), and those that were not strongly connected to Basins (less than five synapses).

The feedforward iLN types received inputs from mechano-ch and made synaptic connections onto both Basin-1 and Basin-2, but differed in the relative number of synapses they made with each (Figure 2B). The iLNa type comprised three hemisegmentally repeated cells that made more synapses onto Basin-2 than Basin-1 (Figure 2B; Data S2). The iLNb type comprised two unpaired medial cells; one made more synapses onto Basin-1 than Basin-2 and the other had equal preference (Figures 2B–2D; Data S2). In contrast to its siblings, Basin-4 received almost no inputs from iLNs downstream of mechano-ch (Figure S2B).

We also identified two GABAergic LNs with specialized feedback (fb) connectivity: fbLN-Ha (Handle-a) and fbLN-Hb (Handle-b). FbLNs received synaptic inputs from Basins (fbLN-Hb also received a small fraction of input from one mechano-ch subtype) and synapsed onto iLNs, but not onto any of the Basins (Figures 2C and S5E–S5G; Data S2). The fbLNs provide a direct pathway for Basins to control the inhibitory circuitry modulating their own activity.

## Reciprocal Inhibition between Feedforward Inhibitory Interneurons that Differentially Inhibit Projection Neurons

The EM connectome revealed complex interactions between the local interneurons in the first-order processing center (Figures 2C, 2E, and 2F). Inhibitory neurons synapsed extensively onto other inhibitory neurons (Figures 2C, 2E, and 2F), with 68% of such connections being reciprocal (Data S2).

iLNa and iLNb made a large number of reciprocal connections with each other (Figures 2E and 2Fiii). Because both neurons directly inhibit Basins, these reciprocal connections could allow iLNa and iLNb neurons to exert a disinhibitory influence on Basin activity patterns. Connectivity suggests that iLNa inhibit Basin-2 and disinhibit Basin-1, while iLNb inhibit Basin-1 and disinhibit Basin-2 (Figures 2E and 2Fii).

Interestingly, the iLNs also form direct connections onto the same neurons that they disinhibit, only with fewer synapses in the direct, than in the disinhibitory pathway (Figures 2E, 2Fii, and 2Fiii). This could prevent output states from becoming too stable and promote output diversity (Liu and Wilson, 2013). The iLNs could also play a dual role in gain control (Carandini and Heeger, 2011; Olsen et al., 2010; Zhu et al., 2013) and in sensorimotor choice.

## A Putative Circuit Motif for Local Feedback Disinhibition of Projection Neurons

The iLNs also received prominent synaptic inputs from the feedback inhibitory interneurons, fbLN-Ha and fbLN-Hb (Figures 2C, 2E, and 2Fiv). The two fbLN-types differed in terms of Basin inputs they received (Figures 2C, 2E, 2Fiv, and S5E–S5G). The fbLN-Ha received many synaptic inputs from all Basins. The fbLN-Hb, received significantly less inputs from Basin-1 than did fbLN-Ha ($p < 0.001$) and it received more inputs from Basin-2 (and Basin-4) than from Basin-1 (Figures 2C, 2E, 2Fiv, and S5E–S5G). Furthermore, fbLNs and iLNs have reciprocal inhibitory connections, which could determine the balance of inhibition and disinhibition of Basin-2 and Basin-1 (Figures 2C, 2E, and 2Fv).

## Synaptic Input from Long-Range Projection Neurons onto Local Inhibitory Interneurons Provides a Pathway for Contextual Modulation of Local Circuitry

Competitive interactions between iLNa and iLNb and fbLNs could promote different patterns of Basin activation, so we asked what factors could contribute to differential activation of the LN-types.

LNs receive differing combinations of mechano-ch inputs (except fbLN-Ha; Data S2), suggesting that distinct combinations of mechano-ch activation could contribute to differential activation of iLNa and iLNb and hence to promoting distinct combinations of Basin PN activity.

EM reconstruction of neurons that make synapses onto iLNs and fbLNs revealed that they also receive input distinct long-range projection neurons from nerve cord and from higher-order brain areas (Figures S5H–S5J). Thus, the LNs integrate local mechanosensory information with other types of contextual or internal state information and the local pattern of Basin activity could be indirectly modulated by contextual and internal state information through control of iLNs.

## A Simple Rate Model Based on the Connectome Explains Behavioral Choice and Behavioral Sequences

To make predictions about the roles of specific circuit motifs, we developed a simple rate model based on the observed connectivity between neuron classes, where weights of excitatory or inhibitory connections between neurons were stronger for connections with more synapses (Figure 3A; see the STAR Methods).

Since different mechano-ch subtypes and contextual input could drive iLNa and iLNb differently, we first asked what output states were produced by the network as a function of iLNa and iLNb activation, while other nodes were driven at constant levels. Since the output is the activity of Basin-1 and Basin-2, we could represent output dynamics as a trajectory in a state space whose two dimensions correspond to Basin-1 and Basin-2 activity (Figure 3B). By sampling from across a landscape of iLNa and iLNb drives (Figure 3C, inset), we found diverse trajectories (Figures 3C and 3D). However, consistent with electrophysiology (Figures 1Q, 1R, and S3C), in all trajectories either Basin-1 was active and Basin-2 was not, or Basin-1 and Basin-2 were co-active. Since trajectories densely occupied only a few regions of Basin state space (Figure 3E), we could define a Basin-state-to-behavior map robust to small changes in the boundaries between behaviors (Figure 3F). Three qualitatively different trajectories resulted from different patterns of iLNa and iLNb drive (Figure 3G): (1) when iLNa was driven weakly, Basin-1 and Basin-2 were co-active across the entire trajectory, corresponding to a bend (Figures 3D and 3H); (2) when iLNa was driven at intermediate levels, output trajectories passed through the Basin-1-on and Basin-2-off state before transitioning to a co-active state, corresponding to a hunch followed by a bend (Figures 3D and 3I); and (3) when iLNa was driven strongly, the dynamics remained in a Basin-1-on and Basin-2-off state, corresponding to a hunch (Figures 3D and 3J).

Thus a simple model of the observed network produced the three most common responses to air puff observed in behaving animals: hunching, bending, and the hunch-bend sequence.

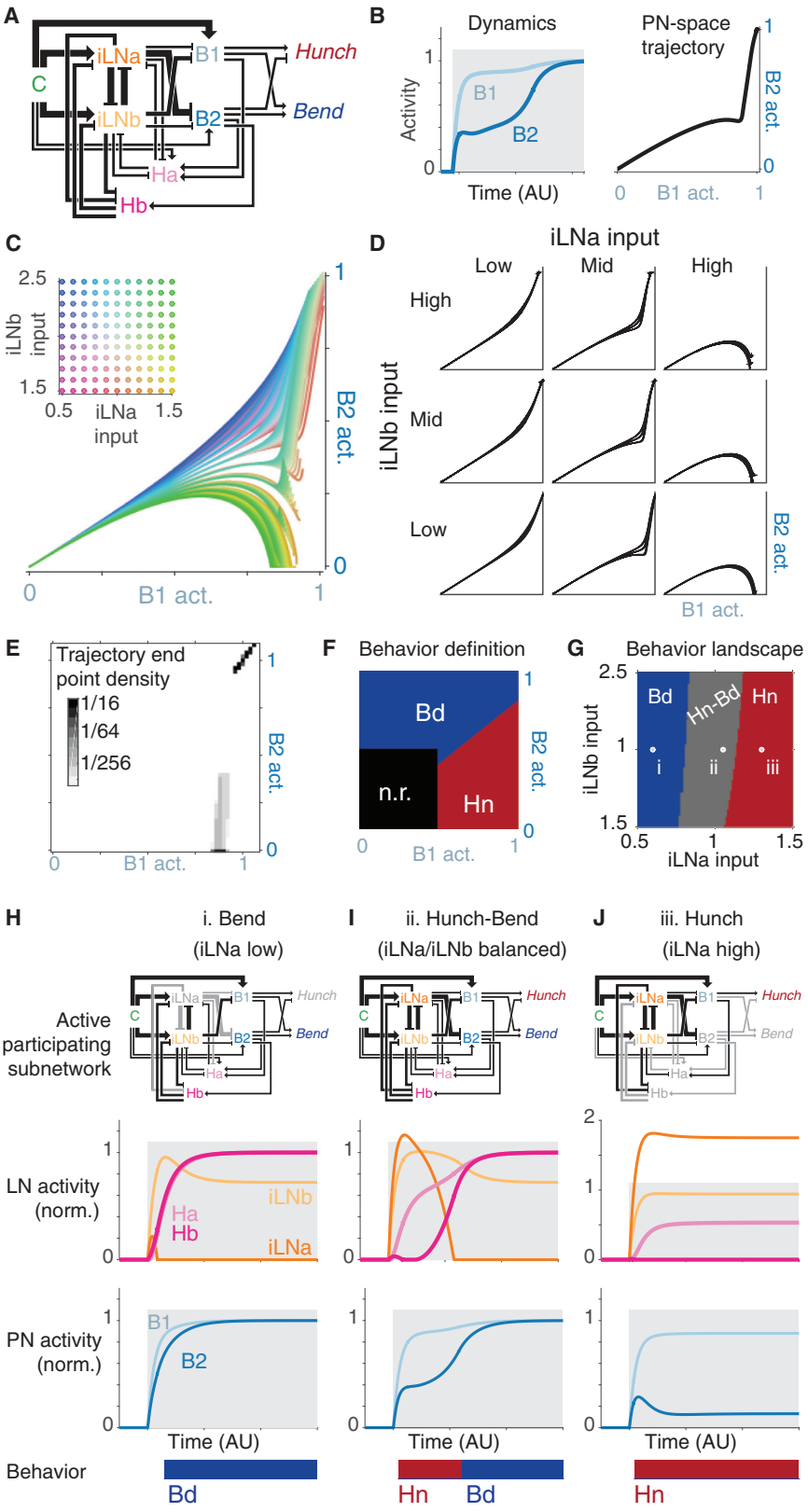


**Figure 3. A Simple Rate Model Based on the Connectome Explains Behavioral Choice and Behavioral Sequences**

(A) Schematic of the network connectivity in a rate model for behavior based on connectivity observed from EM. Line width approximates strength, arrows are excitatory, and squared ends inhibitory. See the STAR Methods for details.

(B) Dynamics of the PN outputs (Basin-1 and Basin-2 activity, left) can be represented as a state space trajectory (right).

(C) Different patterns of sensory input weights onto iLNa and iLNb produce diverse trajectories (colors indicate iLNa; iLNb input values in inset).

(D) Examples of trajectories for different patterns of iLNa and iLNb input for values in the lower one-third, central one-third, and upper one-third of inputs as shown in (C).

(E) Density of trajectory end points, corresponding to dynamical equilibria, for values sampled in C. Note that these fall into two groups, one with Basin-1 activity high and Basin-2 low, the other with both high.

(F) Definition of behavioral response of model as a function of state space. Bd, bend; Hn, hunch; nr, no reaction.

(G) Behavioral landscape as a function of iLNa and iLNb sensory input weights. Pure bending (blue), pure hunching (red), and a hunch-bend sequence (gray) can occur.

(H–J) Examples of dynamics for each behavioral category, corresponding to values labeled by white dots in G. From top to bottom: Active neuron types, interneuronal dynamics, Basin-1 and Basin-2 dynamics, and behavioral output.

(H) Inputs that weakly engage iLNa and preferentially engage the iLNb elements produce co-active Basin output and only a bend state.

(I) Inputs that activate iLNa at intermediate levels and iLNa and iLNb in a balanced manner produce first a high Basin-1 state followed by a co-active state, and thus a hunch-bend sequence.

(J) Inputs that preferentially activate iLNa elements produce a sustained high Basin-1 output and only a hunch state.

See also Figure S6.

### Optogenetic Activation and Intracellular Recordings Confirm Feedforward Disinhibition Predicted by the Connectome-Specified Model

The wiring diagram and the model predict that increasing the activity of iLNa neurons disinhibits Basin-1, promoting a Basin-1-on and Basin-2-off state (hunch), whereas increasing the activity of iLNb neurons disinhibits Basin-2, promoting a co-active state (bend). To test these predictions, we sought to generate Split-GAL4 lines that drive expression selectively in distinct types of iLNs, and LexA-lines that drive expression selectively in individual Basins (Pfeiffer et al., 2010). We managed to generate a Split GAL4-line for an iLNa-type neuron, called Griddle-2 (Figures 4A–4C) and a LexA-line for Basin-1 (see the STAR Methods). With these tools, we could independently target fluorescent labels to Basin-1, while selectively optogenetically activating the iLNa neuron Griddle-2 (Figure 4D), which is synaptically poised to both directly weakly inhibit Basin-1 and indirectly strongly disinhibit Basin-1. Activating Griddle-2 evoked long-latency excitatory postsynaptic responses in Basin-1 (Figures 4E, 4F, and S4T–S4V). This is consistent with a functionally excitatory polysynaptic connection (Fişek and Wilson, 2014; Tuthill and Wilson, 2016) from iLNa to Basin-1, predicted by the wiring diagram (via inhibition of tonic inhibition to Basin-1 provided by iLNb).

### Inactivation of Feedforward Disinhibitory Interneurons Alters Behavioral Choice as Predicted by the Connectome-Specified Model

The model further predicts that selectively activating iLNa-type neurons will inhibit bending and promote hunching (Figure 3J), whereas selectively silencing iLNa-type neurons will promote bending and reduce hunching (Figures 4G–4K). Selective optogenetic activation of Griddle-2 alone significantly reduced bending, but it was not sufficient to trigger hunching (Figure S2F). However, silencing of Griddle-2 significantly reduced the likelihood of hunching and increased bending in response to air puff (Figures 4L–4N). We also analyzed how inactivating Griddle-2 affects the transitions between behaviors. When the larva is not responding to the stimulus it is crawling on the plate, so we included crawling as a third action and computed transition probabilities after stimulus onset in control animals and animals in which Griddle-2 was silenced by TNT. We found that the probabilities of both crawl-to-hunch and bend-to-hunch transitions were significantly reduced in larvae with silenced Griddle-2 neurons (Figures 4O–4Q), indicating Griddle-2 is involved in promoting transitions to hunch.

### Optogenetic Activation and Intracellular Recordings Confirm Feedback Disinhibition Provides a Positive Feedback Loop as Predicted by the Connectome-Specified Model

The wiring diagram and the model predict that fbLN-Hb and fbLN-Ha are activated by Basin-2 and that they in turn promote ramping up of Basin-2 activity via disinhibition, providing a positive feedback loop (Figures 3H–3J and S6A–S6M). To test this prediction, we managed to generate a Split GAL4-line for selectively targeting fbLN-Hb neurons (Figures 5A–5C).

We performed whole-cell patch clamp recording of the GFP-labeled fbLN-Hb in response to optogenetic activation of Basins (Figure 5D). We found that optogenetic activation of Basins evoked short-latency action potentials in fbLN-Hb consistent with a monosynaptic excitatory connection between Basins and fbLNs (Figure 5E).

In converse experiments, we recorded from fluorescently-labeled Basin-1 in response to optogenetic activation of fbLN-Hb (Figures 5F–5H). Activating Handle-b evoked long-latency excitatory postsynaptic responses in Basin-1 in the majority of trials (Figures 5G–5H and S4W–S4Y), consistent with a functionally excitatory polysynaptic connection from dLN to Basin-1 (via inhibition of tonic inhibition to Basin-1 provided by iLNbs). Thus, Basin-2 monosynaptically excites fbLN-Hb, which, in turn, polysynaptically excites and facilitates both Basins, providing a positive feedback loop, as predicted by the wiring-diagram.

### Inactivation of Feedback Disinhibitory Interneurons Alters Behavioral Choice and Sequence as Predicted by the Model

The model predicts that selectively removing fbLN neurons results in decreased activation of Basin-2, thus increasing the likelihood of hunch at the expense of bend (Figures 5I–5M and S6A–S6M). Consistent with this prediction, selective inactivation fbLN-Hb (Figure 5N) resulted in a reduction in bending, and an increase in hunching in response to air puff (Figures 5O and 5P), the opposite phenotype to Griddle-2 inactivation (Figures 4M and 4N). The transition probability from crawl to bend was mildly reduced, while the transition probability from crawl to hunch was increased, consistent with a role in promoting a bend and suppressing a hunch (Figures 5Q–5S). The transition probability from bend back to hunch was also significantly increased when fbLN-Hb was inactivated, suggesting that fbLN-Hb helps prevent the reversal of the hunch-to-bend transition ensuring the maintenance of a bend state.

Taken together, the two inhibitory neurons Griddle-2 and fbLN-Hb promote opposing behaviors: Griddle-2 promotes transitions to a hunch and fbLN-Hb inhibits these transitions. Interestingly, these two inhibitory neurons make reciprocal connections with each other (Figure 2C) through which they could compete for the output state. This connection is asymmetric, however, such that fbLN-Hb makes more synapses onto Griddle-2 than vice versa (Figures 2C, 2E, and 2F; Data S2). We speculate that this could facilitate a progression of the sequence from an initial hunch to bend, but not back to hunch.

### Optogenetic Activation of a Hunch-Promoting PN Evokes Polysynaptic Lateral Excitation of Bend-Promoting Neurons as Predicted by the Model

The model also predicts that activating fbLN-Ha promotes the initiation of sequence transitions from a Basin-1-only state to a co-active state (Figures S6D–S6F and S6M). We could not directly test this role of fbLN-Ha because we lacked a line for targeting expression to fbLN-Ha. However, we confirmed that activating Basin-1 reliably evoked long-latency excitatory responses in Basin-2 that were significantly reduced following application

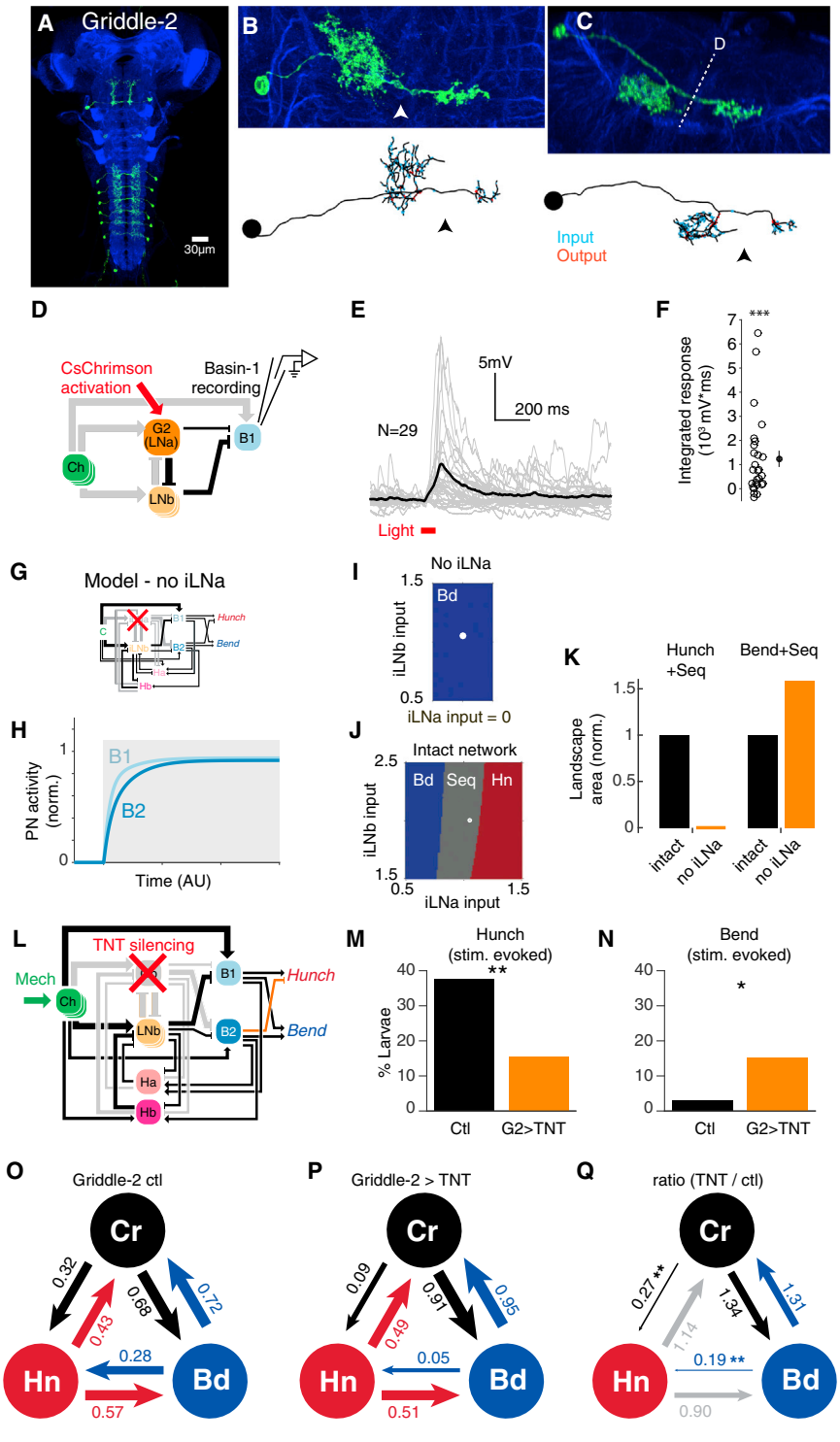


**Figure 4. A Feedforward Inhibitory iLNa Is Functionally Disinhibitory and Alters Behavioral Choice in a Model-Predicted Manner**

(A) Dorsal projection of a confocal stack of split-Gal4 line *JRC-SS0918* driving expression in Griddle-2, an iLNa neuron. Green, *JRC-SS0918-Gal4>UAS-GFP*; blue, N-cadherin staining to indicate neuropil.

(B) Above, dorsal projection of a single Griddle-2 expressing GFP using a FLP-based approach. Below, a Griddle-2 cell reconstructed from EM. Red dashes are output sites; cyan dashes are inputs. Arrowheads indicate midline.

(C) Transverse projections of the cells in (B) (above, light; below, EM). In the light image, the dashed line indicates the midline, dorsal indicated by D.

(D) Schematic for whole-cell recording from Basin-1 and optogenetic activation of Griddle-2 by selective expression of CsChrimson.

(E) Whole-cell recordings of Basin-1 in response to optogenetic activation of Griddle-2. Grey traces represent average of 6–10 trials each for 29 individual animals; black trace represents average across 29 animals. Griddle-2 optogenetic activation evokes long-latency (62 ± 27.8 ms) excitatory responses in Basin-1.

(F) Integrated Basin-1 responses to Griddle-2 activation were positive ($p = 0.000097$, Wilcoxon signed-rank test), indicating depolarization.

(G) Network schematic for model with iLNa silenced.

(H) Model Basin dynamics for parameter values given by a white dot in (I).

(I) The model behavior landscape when iLNa is silenced includes only bends.

(J) Behavioral landscape for the intact network (from Figure 3G).

(K) Area of the behavioral landscape regions producing any hunches (left) or any bends (right) for iLNa silenced, normalized to the intact network.

(L) Network schematic for behavioral assays after silencing Griddle-2 by selective expression of TNT.

(M and N) Percentage of animals performing stimulus-evoked hunching (M) and bending (N) after silencing of Griddle-2 with TNT (orange) and control animals expressing an inactive form of TNT (black). Computation of p value for a difference between stimulus-evoked responses was performed using numerical simulation (see Quantification and statistical analysis in the STAR Methods).

(O–Q) Transition probabilities between crawl, bend, and hunch for control animals (O) and Griddle-2 silenced animals (P). Fisher's exact test was used to compute p values. (Q) The ratio of Griddle-2 silenced to control transition probabilities. (Fisher's exact test; gray indicates no significant change in transitions.)

The number of larvae and exact p values for all the experiments in all figures are specified in Table S1. *$p < 0.05$, **$p < 0.001$ in all figures.

See also Figure S4 and Tables S1 and S3.

of the GABA-A receptor blocker, picrotoxin (Figures 6A–6C). This is consistent with a functionally disinhibitory connection from Basin-1 to Basin-2 and the prediction of the model that fbLN-Ha could promote sequence transitions from Basin-1-only state (hunch) to the co-active state (bend).

## DISCUSSION

We investigated the circuit principles that underlie simple sensorimotor decisions and innate behavioral sequences. By combining large-scale EM reconstruction, connectivity-driven

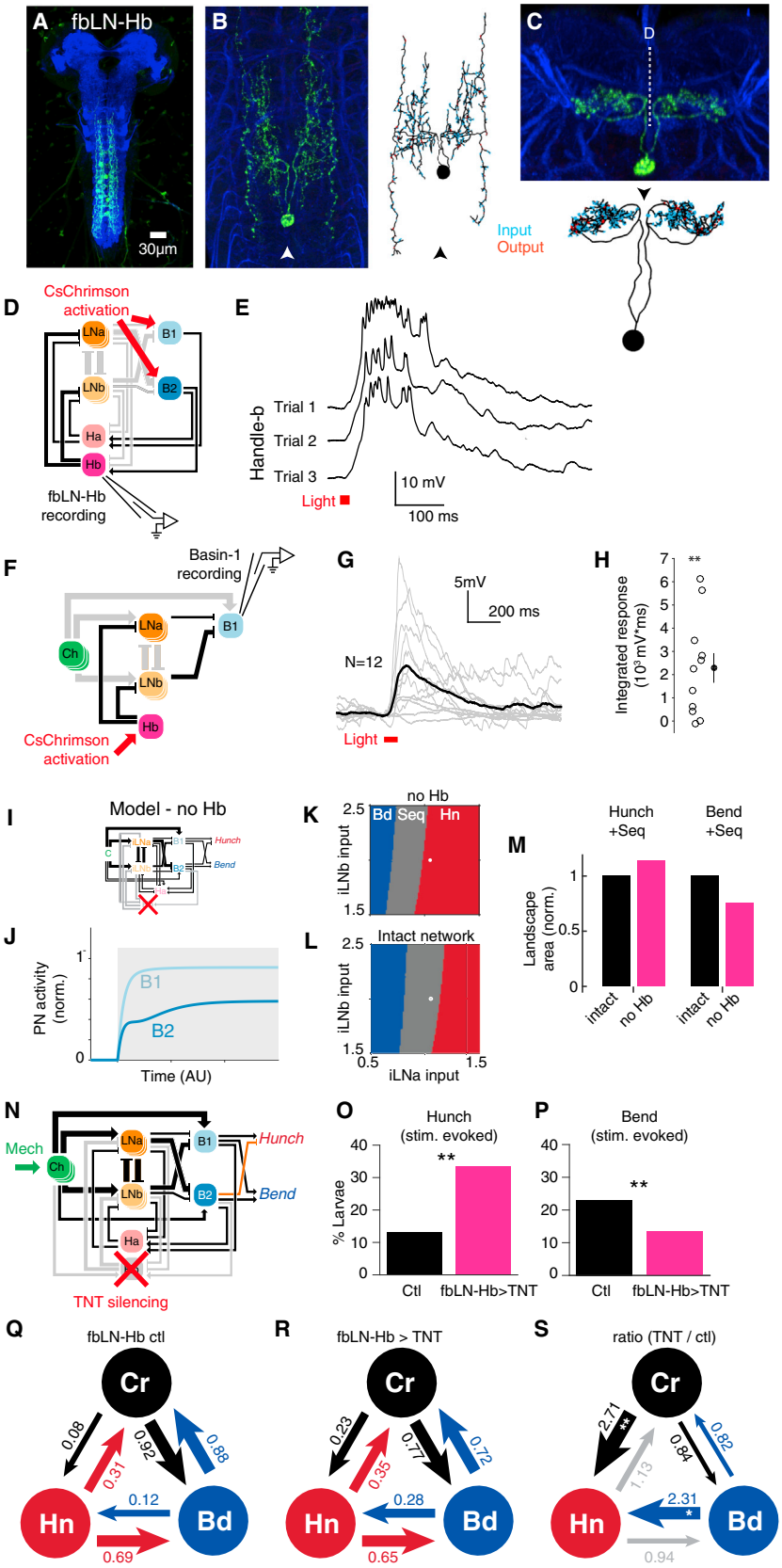


**Figure 5. Feedback fbLN Is Functionally Disinhibitory and Implements Behavioral Choice and Prevents Sequence Transitions in a Model-Predicted Manner**

(A) Dorsal projection of a confocal stack of *JRC-SS0888* driving GFP expression in Hb, an fbLN. Green, *JRC-SS00888-Gal4* > *UAS-GFP*; blue, N-cadherin staining to indicate neuropil.

(B) Left, dorsal projection of a single Hb-expressing GFP using a FLP-based approach. Right, a Hb cell reconstructed from EM. Red dashes are output sites, cyan are inputs. Arrowhead indicates midline.

(C) Transverse projections of the cells in (B) (above, light; below, EM). Note that left and right hemisegmental arbors are connected only via the ventral cell body. In the light image, the dashed line indicates midline with dorsal noted by (D).

(D) Experimental schematic of optogenetic activation of all Basins by targeted expression of CsChrimson during whole-cell recording of Hb.

(E) Whole-cell recordings of Hb in response to optogenetic activation of Basins. Optogenetic activation of Basins reliably evoked short-latency (7.7 ± 3.7 ms) excitatory responses and APs in Hb (15/16 cells).

(F) Network schematic for whole-cell recording from a single Basin-1 and optogenetic activation of Hb by selective expression of CsChrimson.

(G) Whole-cell recordings of Basin-1 in response to optogenetic activation of Hb. Gray traces represent average of 6–10 trials for 12 individual animals; black trace represents average across 12 animals. Optogenetic activation of Hb in the absence of sensory stimulus evoked long-latency (58 – 18.8 ms) excitatory responses in Basin-1.

(H) Integrated Basin-1 responses to Hb activation were positive ($p = 0.008$, Wilcoxon signed-rank test), indicating depolarization.

(I) Network schematic for model without Hb.

(J) Model Basin dynamics for Hb feedback silenced and for parameter values given by a white dot in (K).

(K) Model behavior landscape when Hb is silenced. Dot indicates parameter used in (J).

(L) The model behavior landscape for the intact network.

(M) Area of the behavioral landscape regions producing any hunches (left) or any bends (right) for Hb silenced, normalized to the intact network.

(N) Network schematic for behavioral measurements after silencing Hb by selective expression of TNT.

(O and P) Percentage of animals performing stimulus-evoked hunching (N) and bending (O) in response to air-puff after silencing of Hb with TNT (orange) compared to control (black). Computation of p value for a difference between stimulus-evoked responses was performed using numerical simulation (see Quantification and statistical analysis in the STAR Methods).

(Q–S) Transition probabilities between crawl, bend, and hunch for control animals (P) and Hb-silenced animals (Q). Fisher's exact test was used to compute p values. (S) The ratio of Hb silenced to control transition probabilities (Fisher's exact test. Gray indicates no significant change in transitions).

The number of larvae and exact p values for all the experiments in all figures are specified in Table S1. *$p < 0.05$, **$p < 0.001$ in all figures.

See also Figure S4 and Tables S1 and S3.

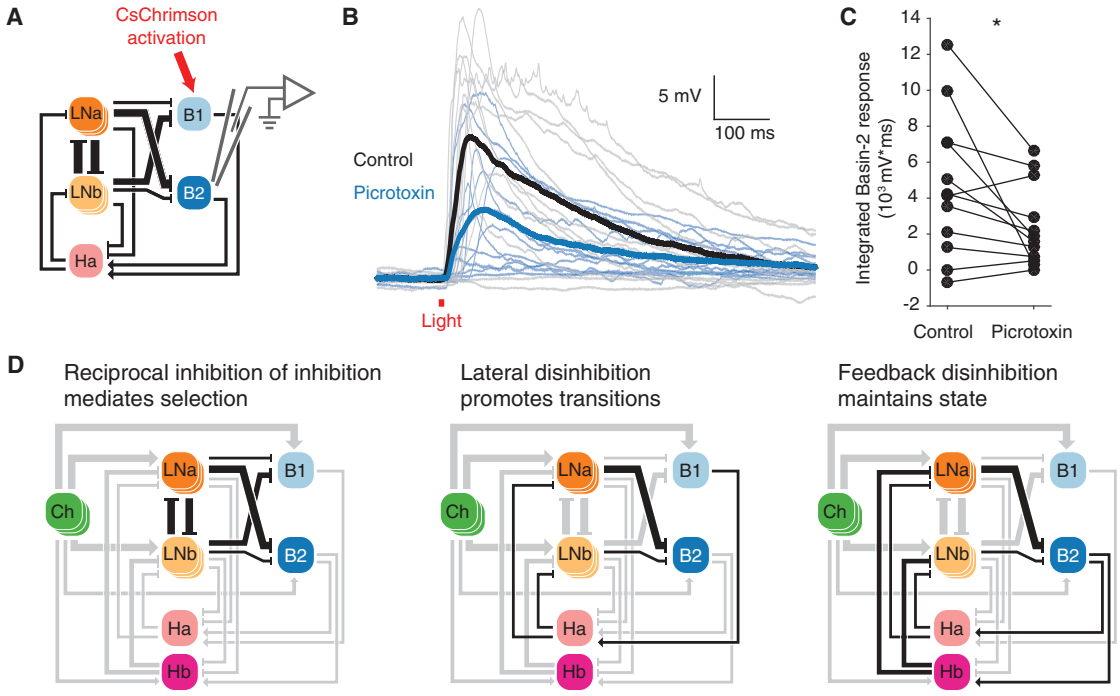


**Figure 6. Optogenetic Activation of Hunch-Promoting PN Produces a Polysynaptic Lateral Excitation of Bend-Promoting PNs**

(A) Experimental schematic for whole-cell intracellular recording of Basin-2 during optogenetic activation of Basin-1.

(B) Basin-1 optogenetic activation evokes long-latency (23 ± 14 ms) depolarizations in Basin-2 (gray). After the application of GABA-A receptor blocker, picrotoxin, (blue) depolarizations were significantly reduced. Thinner traces represent average of 6–10 trials for 11 individual animals; thicker traces represent average across animals.

(C) Integrated depolarization in response to optogenetic activation was significantly reduced by picrotoxin (paired t test, $p = 0.016$).

(D) Network schematics highlighting motifs involved in selection of a behavior, sequence transition and state maintenance.

See also Table S3.

modeling, and behavioral and physiological studies, we identified a three-layer recurrent network in the first-order somatosensory processing center of *Drosophila* larva that contributes to sensorimotor decisions to hunch, bend, or perform a sequence of the two in response to a mechanosensory stimulus. The network consisted of parallel excitatory PNs with differing contributions to behavior, two types of reciprocally connected local feedforward inhibitory interneurons that preferentially targeted distinct PNs, and disinhibitory feedback interneurons directly downstream of the PNs that are reciprocally connected with the feedforward inhibitory interneurons. Our findings are consistent with a model in which reciprocal inhibition between the feedforward inhibitory interneurons implements selection, while feedback disinhibition stabilizes the selection and lateral disinhibition promotes transitions from the first behavior to the next one (Figure S6D).

## Reciprocally Connected Feedforward Inhibitory Interneurons Implement Behavioral Choice

Local or long-range feedforward disinhibition has been implicated in gating behaviors and percepts in several systems. In the basal ganglia, the direct pathway disinhibits specific actions via two sequential layers of GABAergic projection neurons (Mink, 1996). In visual and auditory cortex in mice, a specialized class of GABAergic interneurons target other GABAergic interneurons, disinhibiting excitatory pyramidal cells to increase excitatory gain based on behavioral context (Fu et al., 2014; Pfeffer et al., 2013; Zhang et al., 2014) or reinforcement signals (Hangya et al., 2014; Kepecs and Fishell, 2014; Pi et al., 2013). In amygdala, distinct disinhibitory circuits driven by painful stimuli or auditory cues enhance fear conditioning (Wolff et al., 2014). Recent studies in the adult and larval fly brain revealed feedforward disinhibitory motifs in thermosensory (Liu et al., 2015) and olfactory centers (Berck et al., 2016; Liu and Wilson, 2013).

In the above systems, disinhibition is asymmetric, i.e., one interneuron type inhibits another, thus gating a specific percept or action, but does not receive strong inhibition in return. Our EM reconstruction revealed extensive reciprocal connectivity that suggests competitive interactions between classes of disinhibitory interneurons. Reciprocal connections between inhibitory neurons have been observed in several brain areas in vertebrates, including tectum (Goddard et al., 2014), cortex (Pfeffer et al., 2013) and striatum (Mink, 1996), as well as in insects (Liu and Wilson, 2013). In theoretical models, the reciprocal inhibition of inhibition can be used to implement winner-take-all decisions (Goddard et al., 2014; Mysore and Knudsen, 2012; Mysore et al., 2011; Redgrave et al., 2011; Sridharan and Knudsen, 2015). However, the exact identity and the roles of

reciprocally connected interneurons in behavior have been harder to decipher. Here, we demonstrated that interneurons involved in promoting distinct behaviors via disinhibition have extensive reciprocal connections. Specifically, Griddle-2 neurons, which promote hunch and suppress bend, make reciprocal GABAergic synapses with the fbLN-Hb, which suppress hunch and promote bend.

### Feedback Disinhibition Provides Positive Feedback for Stabilizing Behavioral Choice

Recurrent excitation between neurons that promote the same choice can play a key role in models of behavioral choice by stabilizing decisions and allowing slow integration of inputs (Wang, 2008). In cortex, recurrent excitatory connections have been found between neurons that have similar visual tuning properties (Harris and Mrsic-Flogel, 2013). In male *Caenorhabditis* elegans, recurrent excitatory connections are found between sensory neurons in a circuit mediating behavioral choice (Jarrell et al., 2012). We find a different functionally positive recurrent motif: feedback disinhibition. We showed that feedback disinhibition maintains a selected behavior and prevents transitions to earlier behaviors in a sequence. The advantage of feedback disinhibition over recurrent excitation could be that the circuit remains sensitive to sensory input as the primary source of excitation, and thus can quickly respond to changes in stimulus. In addition, disinhibitory neurons have the simultaneous ability to both promote one state and inhibit opposing states. Indeed, the feedback fbLN involved in inhibiting hunching and promoting bending have extensive reciprocal GABAergic connections with feedforward iLNa that inhibit the behavior fbLN promote and that promote the behavior the dLN inhibit.

### Lateral Disinhibition Can Promote Sequence Transitions

Our study provides insight into the mechanisms of generating behavioral sequences. Some highly stereotyped sequential behaviors are well described by "synfire-chain" models which propose that each element in a series of actions provides the excitation of the next (Long et al., 2010). Probabilistic sequences, such as human typing or fly grooming, are better described by competitive queuing models which propose all actions in a sequence are readied in parallel and the order is established through gradients of excitation and mutual inhibitory interactions (Rosenbaum et al., 2007; Seeds et al., 2014). In line with the competitive queuing model architecture, we find projection neurons that promote or inhibit distinct behaviors are targeted in parallel by mechanosensory neurons. A mechanosensory stimulus can activate either the bend-promoting activity pattern (Basin-1 and Basin-2 co-active) or the hunch-promoting activity pattern (Basin-1-on, Basin-2-off). However, the lateral disinhibitory neuron fbLN-Ha participates in a motif similar to a synfire chain. Based on connectivity (Figures 2B–2F and S5E–S5G), this neuron can be activated by PNs that promote the hunch, and it can disinhibit PNs that promote bending and inhibit hunching. In this way, fbLN-Ha can promote the initiation of the hunch-bend sequence transitions (Figures 3, 6, and S6). Feedback disinhibition mediated by both, fbLN-Ha and the related fbLN-Hb, "traps" the second state and prevents reversals back to the first one (Figures 3, 6, and S6). Chains of lateral disinhibitory connections acting to sequentially gate behaviors could be a general mechanism underlying flexible sequence transitions in other systems.

### Pathway for Contextual Modulation of Local Circuitry

EM reconstruction revealed that iLNa, iLNb, and fbLNs receive inputs from distinct subsets of local mechano-ch neurons as well as from distinct long-range PNs carrying information from the brain or from other distant body regions. This suggests the outcomes of competitive interactions between the LN-types depend both on precise patterns of local activation of mechano-ch neurons as well as on broader contextual and internal state information provided by the long-range projection neurons. Extrasynaptic neuromodulation not detectable using EM reconstruction could also be present (Marder, 2012).

### Complex Inhibitory Interneuron Networks at the Earliest Stages of Sensory Processing Enable Efficient and Dynamic Implementation of Behavioral Choice

Our results revealed a combination of multiple interconnected motifs in the first-order somatosensory circuit of *Drosophila* larva, each normally proposed in distinct theoretical models of decision making in higher order brain areas in higher animals. The distribution of behavioral choice and choice-related activity across sensorimotor pathways (Nienborg et al., 2012; Yang et al., 2016) has been proposed within the non-hierarchical framework of decision-making to be a more rapid and flexible mechanism for incorporating internal, proprioceptive, and environmental context (Cisek and Kalaska, 2010). The circuit described here is well-suited to operating in such a rich manner: implementing sensorimotor decisions and behavioral sequences at the earliest stages of sensory processing while also possessing pathways for contextual modulation, allowing for decisions to be made in a dynamic and ongoing interaction with the environment.

## STAR★METHODS

Detailed methods are provided in the online version of this paper and include the following:

- KEY RESOURCES TABLE
- CONTACT FOR REAGENTS AND RESOURCE SHARING
- EXPERIMENTAL MODEL AND SUBJECT DETAILS
  - Fly Stocks
- METHOD DETAILS
  - Behavioral Apparatus
  - Behavioral Experiments
  - Mechanical and Optogenetic Stimulation for Electrophysiology Recordings
  - Whole-Cell Patch-Clamp Recordings from Basin Neurons in Ventral Nerve Cord
  - Basin Neuron Identification
  - Spike Detection in Electrophysiological Recordings of Basin Neurons
  - GABA Histochemistry Labeling
  - EM Reconstruction and Wiring Diagrams
  - Model

## SUPPLEMENTAL INFORMATION

Supplemental Information includes six figures, three tables, and two data and can be found with this article online at http://dx.doi.org/10.1016/j.cell.2016.09.009.

## AUTHOR CONTRIBUTIONS

T.J., C.M.S.-M., A.C., and M.Z. conceived the experiments and wrote the manuscript. T.J., and M.S. performed the experiments. T.J., M.S., and C.M.S.-M. analyzed the data. C.S.M. performed EM reconstructions, network analysis, and modeling. G.D. and J.-B.M. provided behavior detection methodology. J.W.T and R.D.F. provided reagents. B.D.M. provided feedback for writing.

## ACKNOWLEDGMENTS

We thank G. Rubin and the Janelia Fly EM Project for the gift of the comprehensive EM dataset of the larval nervous system (for EM); B. Arruda and T. Dang for assistance with behavioral screens; G. Rubin, H. Dionne, and B. Pfeiffer for GAL4 and Split GAL4 lines; J. Simpson for sharing the UAS-impTNT unpublished stock, V. Jayaraman for sharing 20xUAS-CsChrimson-mCherry-trafficked in su(Hw)attP1 unpublished stock; and the GENIE project (JANELIA, HHMI) for sharing the 13xLexAop2-IVS-GCaMP6s-p10 50.641 in VK000005 unpublished stock. We thank A. Nern and G. Rubin for the single-cell FLP-out stocks; H.-H. Li, O. Malkesman, and Janelia Fly Light Project Team for images of neuronal lines; K. Hibbard, M. Mercer, T. Laverty, and the rest of Janelia Fly Core for stock construction and fly crosses; E. Trautman, R. Svirskas, C. Weaver, Lowell Umayam, and D. Olbris for data analysis pipelines; and C. Priebe for advice on the statistical analysis. We thank Chris Doe, Misha Ahrens, and Maarten Zwart for critically reading the manuscript. We thank Janelia HHMI for funding.

Received: May 9, 2016
Revised: August 3, 2016
Accepted: September 6, 2016
Published: October 6, 2016

## REFERENCES

Baca, S.M., Marin-Burgin, A., Wagenaar, D.A., and Kristan, W.B., Jr. (2008). Widespread inhibition proportional to excitation controls the gain of a leech behavioral circuit. Neuron *57*, 276–289.

Barker, A.J., and Baier, H. (2015). Sensorimotor decision making in the zebrafish tectum. Curr. Biol. *25*, 2804–2814.

Berck, M.E., Khandelwal, A., Claus, L., Hernandez-Nunez, L., Si, G., Tabone, C.J., Li, F., Truman, J.W., Fetter, R.D., Louis, M., et al. (2016). The wiring diagram of a glomerular olfactory system. Elife *13*, 5.

Bishop, C. (2006). Pattern Recognition and Machine Learning (Springer).

Breiman, L. (2001). Random Forest. Mach. Learn. *45*, 5–32.

Briggman, K.L., and Kristan, W.B., Jr. (2006). Imaging dedicated and multifunctional neural circuits generating distinct behaviors. J. Neurosci. *26*, 10925–10933.

Briggman, K.L., Abarbanel, H.D.I., and Kristan, W.B., Jr. (2005). Optical imaging of neuronal populations during decision-making. Science *307*, 896–901.

Bullock, D. (2004). Adaptive neural models of queuing and timing in fluent action. Trends Cogn. Sci. *8*, 426–433.

Burrows, M., and Siegler, M.V. (1976). Transmission without spikes between locust interneurones and motoneurones. Nature *262*, 222–224.

Carandini, M., and Heeger, D.J. (2011). Normalization as a canonical neural computation. Nat. Rev. Neurosci. *13*, 51–62.

Chen, T.-W., Wardill, T.J., Sun, Y., Pulver, S.R., Renninger, S.L., Baohan, A., Schreiter, E.R., Kerr, R.A., Orger, M.B., Jayaraman, V., et al. (2013). Ultrasensitive fluorescent proteins for imaging neuronal activity. Nature *499*, 295–300.

Cisek, P. (2007). Cortical mechanisms of action selection: the affordance competition hypothesis. Philos. Trans. R. Soc. Lond. B Biol. Sci. *362*, 1585–1599.

Cisek, P., and Kalaska, J.F. (2010). Neural mechanisms for interacting with a world full of action choices. Annu. Rev. Neurosci. *33*, 269–298.

Cui, G., Jun, S.B., Jin, X., Pham, M.D., Vogel, S.S., Lovinger, D.M., and Costa, R.M. (2013). Concurrent activation of striatal direct and indirect pathways during action initiation. Nature *494*, 238–242.

Fişek, M., and Wilson, R.I. (2014). Stereotyped connectivity and computations in higher-order olfactory neurons. Nat. Neurosci. *17*, 280–288.

Fu, Y., Tucciarone, J.M., Espinosa, J.S., Sheng, N., Darcy, D.P., Nicoll, R.A., Huang, Z.J., and Stryker, M.P. (2014). A cortical circuit for gain control by behavioral state. Cell *156*, 1139–1152.

Gaudry, Q., and Kristan, W.B., Jr. (2009). Behavioral choice by presynaptic inhibition of tactile sensory terminals. Nat. Neurosci. *12*, 1450–1457.

Goddard, C.A., Mysore, S.P., Bryant, A.S., Huguenard, J.R., and Knudsen, E.I. (2014). Spatially reciprocal inhibition of inhibition within a stimulus selection network in the avian midbrain. PLoS ONE *9*, e85865.

Gomez-Marin, A., Stephens, G.J., and Louis, M. (2011). Active sampling and decision making in Drosophila chemotaxis. Nat. Commun. *2*, 441.

Gordus, A., Pokala, N., Levy, S., Flavell, S.W., and Bargmann, C.I. (2015). Feedback from network states generates variability in a probabilistic olfactory circuit. Cell *161*, 215–227.

Gouwens, N.W., and Wilson, R.I. (2009). Signal propagation in Drosophila central neurons. J. Neurosci. *29*, 6239–6249.

Hangya, B., Pi, H.-J., Kvitsiani, D., Ranade, S.P., and Kepecs, A. (2014). From circuit motifs to computations: mapping the behavioral repertoire of cortical interneurons. Curr. Opin. Neurobiol. *26*, 117–124.

Harris, K.D., and Mrsic-Flogel, T.D. (2013). Cortical connectivity and sensory coding. Nature *503*, 51–58.

Hengstenberg, R. (1977). Spike responses of 'non-spiking' visual interneurone. Nature *270*, 338–340.

Hikosaka, O., Takikawa, Y., and Kawagoe, R. (2000). Role of the basal ganglia in the control of purposive saccadic eye movements. Physiol. Rev. *80*, 953–978.

Jarrell, T.A., Wang, Y., Bloniarz, A.E., Brittin, C.A., Xu, M., Thomson, J.N., Albertson, D.G., Hall, D.H., and Emmons, S.W. (2012). The connectome of a decision-making neural network. Science *337*, 437–444.

Kepecs, A., and Fishell, G. (2014). Interneuron cell types are fit to function. Nature *505*, 318–326.

Kernan, M., Cowan, D., and Zuker, C. (1994). Genetic dissection of mechanosensory transduction: mechanoreception-defective mutations of Drosophila. Neuron *12*, 1195–1206.

Klapoetke, N.C., Murata, Y., Kim, S.S., Pulver, S.R., Birdsey-Benson, A., Cho, Y.K., Morimoto, T.K., Chuong, A.S., Carpenter, E.J., Tian, Z., et al. (2014). Independent optical excitation of distinct neural populations. Nat. Methods *11*, 338–346.

Kovac, M.P., and Davis, W.J. (1977). Behavioral choice: neural mechanisms in Pleurobranchaea. Science *198*, 632–634.

Kristan, W.B. (2008). Neuronal decision-making circuits. Curr. Biol. *18*, R928–R932.

Kristan, W.B. (2014). Behavioral sequencing: competitive queuing in the fly CNS. Curr. Biol. *24*, R743–R746.

Lahiri, S., Shen, K., Klein, M., Tang, A., Kane, E., Gershow, M., Garrity, P., and Samuel, A.D.T. (2011). Two alternating motor programs drive navigation in Drosophila larva. PLoS ONE *6*, e23180.

Lasley, K.S. (1951). The Problem of Serial Order in Behavior (Wiley).

Li, H.-H., Kroll, J.R., Lennox, S.M., Ogundeyi, O., Jeter, J., Depasquale, G., and Truman, J.W. (2014). A GAL4 driver resource for developmental and behavioral studies on the larval CNS of Drosophila. Cell Rep. *8*, 897–908.

Liu, W.W., and Wilson, R.I. (2013). Glutamate is an inhibitory neurotransmitter in the Drosophila olfactory system. Proc. Natl. Acad. Sci. USA *110*, 10294–10299.

Liu, W.W., Mazor, O., and Wilson, R.I. (2015). Thermosensory processing in the Drosophila brain. Nature *519*, 353–357.

Long, M.A., Jin, D.Z., and Fee, M.S. (2010). Support for a synaptic chain model of neuronal sequence generation. Nature *468*, 394–399.

Marder, E. (2012). Neuromodulation of neuronal circuits: back to the future. Neuron *76*, 1–11.

Milde, J. (1981). Graded potentials and action potentials in the large ocellar interneurons of the bee. J. Comp. Physiol. *143*, 427–434.

Mink, J.W. (1996). The basal ganglia: focused selection and inhibition of competing motor programs. Prog. Neurobiol. *50*, 381–425.

Mysore, S.P., and Knudsen, E.I. (2012). Reciprocal inhibition of inhibition: a circuit motif for flexible categorization in stimulus selection. Neuron *73*, 193–205.

Mysore, S.P., Asadollahi, A., and Knudsen, E.I. (2011). Signaling of the strongest stimulus in the owl optic tectum. J. Neurosci. *31*, 5186–5196.

Nern, A., Pfeiffer, B.D., and Rubin, G.M. (2015). Optimized tools for multicolor stochastic labeling reveal diverse stereotyped cell arrangements in the fly visual system. Proc. Natl. Acad. Sci. USA *112*, E2967–E2976.

Nienborg, H., Cohen, M.R., and Cumming, B.G. (2012). Decision-related activity in sensory neurons: correlations among neurons and with behavior. Annu. Rev. Neurosci. *35*, 463–483.

Ohyama, T., Jovanic, T., Denisov, G., Dang, T.C., Hoffmann, D., Kerr, R.A., and Zlatic, M. (2013). High-throughput analysis of stimulus-evoked behaviors in Drosophila larva reveals multiple modality-specific escape strategies. PLoS ONE *8*, e71706.

Ohyama, T., Schneider-Mizell, C.M., Fetter, R.D., Aleman, J.V., Franconville, R., Rivera-Alba, M., Mensh, B.D., Branson, K.M., Simpson, J.H., Truman, J.W., et al. (2015). A multilevel multimodal circuit enhances action selection in Drosophila. Nature *520*, 633–639.

Olsen, S.R., Bhandawat, V., and Wilson, R.I. (2010). Divisive normalization in olfactory population codes. Neuron *66*, 287–299.

Pearson, K.G. (1976). Nerve cells without action potentials. In Simpler Networks and Behaviors, J.C. Fentress, ed. (Sinuear Associates), pp. 99–110.

Pfeffer, C.K., Xue, M., He, M., Huang, Z.J., and Scanziani, M. (2013). Inhibition of inhibition in visual cortex: the logic of connections between molecularly distinct interneurons. Nat. Neurosci. *16*, 1068–1076.

Pfeiffer, B.D., Jenett, A., Hammonds, A.S., Ngo, T.-T.B., Misra, S., Murphy, C., Scully, A., Carlson, J.W., Wan, K.H., Laverty, T.R., et al. (2008). Tools for neuroanatomy and neurogenetics in Drosophila. Proc. Natl. Acad. Sci. USA *105*, 9715–9720.

Pfeiffer, B.D., Ngo, T.-T.B., Hibbard, K.L., Murphy, C., Jenett, A., Truman, J.W., and Rubin, G.M. (2010). Refinement of tools for targeted gene expression in Drosophila. Genetics *186*, 735–755.

Pfeiffer, B.D., Truman, J.W., and Rubin, G.M. (2012). Using translational enhancers to increase transgene expression in Drosophila. Proc. Natl. Acad. Sci. USA *109*, 6626–6631.

Pi, H.-J., Hangya, B., Kvitsiani, D., Sanders, J.I., Huang, Z.J., and Kepecs, A. (2013). Cortical interneurons that specialize in disinhibitory control. Nature *503*, 521–524.

Redgrave, P., Vautrelle, N., and Reynolds, J.N.J. (2011). Functional properties of the basal ganglia's re-entrant loop architecture: selection and reinforcement. Neuroscience *198*, 138–151.

Rosenbaum, D.A., Cohen, R.G., Jax, S.A., Weiss, D.J., and van der Wel, R. (2007). The problem of serial order in behavior: Lashley's legacy. Hum. Mov. Sci. *26*, 525–554.

Saalfeld, S., Cardona, A., Hartenstein, V., and Tomancak, P. (2009). CATMAID: collaborative annotation toolkit for massive amounts of image data. Bioinformatics *25*, 1984–1986.

Schneider-Mizell, C.M., Gerhard, S., Longair, M., Kazimiers, T., Li, F., Zwart, M.F., Champion, A., Midgley, F.M., Fetter, R.D., Saalfeld, S., and Cardona, A. (2016). Quantitative neuroanatomy for connectomics in Drosophila. eLife *5*, 1133.

Seeds, A.M., Ravbar, P., Chung, P., Hampel, S., Midgley, F.M., Jr., Mensh, B.D., and Simpson, J.H. (2014). A suppression hierarchy among competing motor programs drives sequential grooming in Drosophila. eLife *3*, e02951.

Sridharan, D., and Knudsen, E.I. (2015). Selective disinhibition: A unified neural mechanism for predictive and post hoc attentional selection. Vision Res. *116* (Pt B), 194–209.

Struhl, G., and Basler, K. (1993). Organizing activity of wingless protein in Drosophila. Cell *72*, 527–540.

Sweeney, S.T., Broadie, K., Keane, J., Niemann, H., and O'Kane, C.J. (1995). Targeted expression of tetanus toxin light chain in Drosophila specifically eliminates synaptic transmission and causes behavioral defects. Neuron *14*, 341–351.

Swierczek, N.A., Giles, A.C., Rankin, C.H., and Kerr, R.A. (2011). High-throughput behavioral analysis in C. elegans. Nat. Methods *8*, 592–598.

Tsubouchi, A., Caldwell, J.C., and Tracey, W.D. (2012). Dendritic filopodia, Ripped Pocket, NOMPC, and NMDARs contribute to the sense of touch in Drosophila larvae. Curr. Biol. *22*, 2124–2134.

Tuthill, J.C., and Wilson, R.I. (2016). Parallel transformation of tactile signals in central circuits of Drosophila. Cell *164*, 1046–1059.

von Reyn, C.R., Breads, P., Peek, M.Y., Zheng, G.Z., Williamson, W.R., Yee, A.L., Leonardo, A., and Card, G.M. (2014). A spike-timing mechanism for action selection. Nat. Neurosci. *17*, 962–970.

Vogelstein, J.T., Park, Y., Ohyama, T., Kerr, R.A., Truman, J.W., Priebe, C.E., and Zlatic, M. (2014). Discovery of brainwide neural-behavioral maps via multiscale unsupervised structure learning. Science *344*, 386–392.

Wang, X.-J. (2008). Decision making in recurrent neuronal circuits. Neuron *60*, 215–234.

Wolff, S.B.E., Gründemann, J., Tovote, P., Krabbe, S., Jacobson, G.A., Müller, C., Herry, C., Ehrlich, I., Friedrich, R.W., Letzkus, J.J., and Lüthi, A. (2014). Amygdala interneuron subtypes control fear learning through disinhibition. Nature *509*, 453–458.

Yang, H., Kwon, S.E., Severson, K.S., and O'Connor, D.H. (2016). Origins of choice-related activity in mouse somatosensory cortex. Nat. Neurosci. *19*, 127–134.

Zhang, W., Yan, Z., Jan, L.Y., and Jan, Y.-N. (2013). Sound response mediated by the TRP channels NOMPC, NANCHUNG, and INACTIVE in chordotonal organs of Drosophila larvae. Proc. Natl. Acad. Sci. USA *110*, 13612–13617.

Zhang, S., Xu, M., Kamigaki, T., Hoang Do, J.P., Chang, W.C., Jenvay, S., Miyamichi, K., Luo, L., and Dan, Y. (2014). Selective attention. Long-range and local circuits for top-down modulation of visual cortex processing. Science *345*, 660–665.

Zhu, P., Frank, T., and Friedrich, R.W. (2013). Equalization of odor representations by a network of electrically coupled inhibitory interneurons. Nat. Neurosci. *16*, 1678–1686.

## STAR★METHODS

### KEY RESOURCES TABLE

| REAGENT or RESOURCE | SOURCE | IDENTIFIER |
|---|---|---|
| Antibodies | | |
| Anti-GABA antibody produced in rabbit | Sigma-Aldrich | A2052; RRID: AB_477652 |
| Anti-GFP antibody produced in chicken | Abcam | Ab13970; RRID: AB_300798 |
| Goat anti-chicken secondary antibody Alexa Fluor 488 | Invitrogen | A11039; RRID: AB_142924 |
| Goat anti-rabbit IgG secondary antibody Alexa Fluor 647 | Invitrogen | A21244; RRID: AB_141663 |
| Chemicals, Peptides, and Recombinant Proteins | | |
| picrotoxin | Sigma-Aldrich | P-1675; CAS 124-87-8 |
| All-trans-retinal | TRC Canada (Toronto research chemicals inc) | Cat #: R240000 |
| Protease from *Streptomyces griseus* Type XIV | Sigma-Aldrich | A-5147; CAS 9036-06-0 |
| Experimental Models: Organisms/Strains | | |
| Drosophila, pJFRC12-10XUAS-IVS-myr::GFP | Bloomington | 32197 |
| Drosophila, 20xUAS-CsChrimson-mVenus trafficked in attP18 | Bloomington | 55134 |
| Drosophila, UAS-impTNT (II) | Julie Simpson, unpiblished | This paper |
| Drosophila, 20B01-LexAp65 (JK22c); 20xUAS-CsChrimson-mCherry-trafficked in su(Hw)attP1, 13xLexAop2-IVS-GCaMP6s-p10 50.641 in VK5 | | This paper |
| Drosophila, R72F11-p65ADZp in attP40; R38H09-ZpGdbd in attP2 (JRC-SS00739), UAS-GCamp6f 15.693 in VK0005 | | This paper |
| Drosophila, w;20B01-LexA/CyO;13Lexop2 myr:: TDTomato/MKRS | | This paper |
| Drosophila, 20xUAS-CsChrimson-mCherry-trafficked in su(Hw)attP1 | Gift from Vivek Jayaraman, unpublished stock | This paper |
| Drosophila, 13xLexAop2-IVS-GCaMP6s-p10 50.641 in VK000005 | Gift from GENIE project (JRC, HHMI), unpublished stock | This paper |
| Drosophila, LexAop2-myr::TDTomato-p10 (attp40) | Gift from D. Mellert | Ohyama et al., 2015 |
| Drosophila, pGP-20XUAS-GCaMP6f-p10.92.693 in VK00005 | Gift from GENIE project (JRC, HHMI), unpublished stock | This paper |
| Drosophila, UAS-TNT-e | | Sweeney et al., 1995 |
| Drosophila, w;;attp2 | Gift from G.Rubin | Pfeiffer et al., 2008; 2010) |
| Drosophila, w;attP40;attP2 | Gift from G.Rubin | Pfeiffer et al., 2010 |
| Drosophila, R61D08-GAL4 | Bloomington | 39272, Pfeiffer et al., 2008 |
| Drosophila, R21B01-GAL4 | Bloomington | 48877, Pfeiffer et al., 2008 |
| Drosophila, R72F11-GAL4 | Bloomington | 39786, Pfeiffer et al., 2008 |
| Drosophila, R36B06-GAL4 | Bloomington | 49929, Pfeiffer et al., 2008 |
| Drosophila, R16B12-GAL4 | Gift from G.Rubin | Pfeiffer et al., 2008 |
| Drosophila, R21B01-LexA | Bloomington | 52558 |
| Drosophila, RC-SS00739 | | This paper |
| Drosophila, RC-SS00888 | | This paper |
| Drosophila, RC-SS00918 | | This paper |
| Drosophila, RC-SS00863 | | This paper |
| Drosophila, JRC-SS00674 | | This paper |
| Drosophila, JRC-SS00740 | | Ohyama et al., 2015 |
| Software and Algorithms | | |
| pCLAMP | Molecular Devices | pCLAMP 10 |
| MWT (multiworm tracker) | http://sourceforge.net/projects/mwt | Swierczek et al., 2011 |

(*Continued on next page*)

*Continued*

| REAGENT or RESOURCE | SOURCE | IDENTIFIER |
|---|---|---|
| LARA software package | http://sourceforge.net/projects/salam-hhmi | Ohyama et al., 2013 |
| CATMAID | http://www.catmaid.org | Saalfeld et al., 2009, Schneider-Mizell et al., 2016 |
| MATLAB | http://www.mathworks.org | |

## CONTACT FOR REAGENTS AND RESOURCE SHARING

Further information and requests for reagents may be directed to, and will be fulfilled by the corresponding authors Dr. Marta Zlatic (zlaticm@janelia.hhmi.org) and Dr. Albert Cardona (cardonaa@janelia.hhmi.org).

## EXPERIMENTAL MODEL AND SUBJECT DETAILS

### Fly Stocks

In the main text and figures, short names are used to describe genotypes for clarity. The complete genotypes of animals used in this study are shown in Table S3. We used GAL4-UAS system to direct the expression of effector proteins to specific neuron subtypes. We used UAS-TNT-e (Sweeney et al., 1995) to silence neurons by expressing the tetanus toxin light chain in the GAL4 and Split GAL4 lines we tested, pJFRC12-10XUAS-IVS-myr::GFP (Bloomington stocknumber: 32197 gift from B. D. Pfeiffer, G. Rubin and the GENIE project team (HHMI Janelia Research Campus) to label neurons with green fluorescence and 20xUAS-CsChrimson-mVenus trafficked in attP18 (Bloomington stocknumber: 55134) to activate neurons. Throughout the paper we used as controls the progeny larvae from the UAS-impTNT (II) (gift from J. Simpson, unpublished data) containing the inactive form of TNT (Sweeney et al., 1995), crossed to appropriate GAL4 or Split GAL4 lines. We used the progeny larvae from the insertion site stock, w;;attp2, w;attP40;attP2 (Pfeiffer et al., 2010; 2008) crossed to the appropriate effector (UAS-TNT-e (II)) for characterizing the behavior (in Figures 1 and S1). w;; attP2 and w;attP40;attP2 were selected because they have the same genetic background as the GAL4 and Split Gal4 lines tested respectively. The following strains from the Rubin GAL4/LexA collection were used for the behavioral experiments, immunohistochemistry labeling, flp-out experiments and electrophysiological recordings in the manuscript: R61D08-GAL4, R21B01-GAL4, R72F11-GAL4, R36B06-GAL4, R16B12-GAL4, R21B01-LexA (Li et al., 2014). To selectively target Basin-2 neurons we generated a Split-GAL4 stock: R72F11_AD inserted in attp40 (chromosome 2L) and R38H09_DBD

in attp2 (3L) (JRC-SS00739). To selectively target Handle-B neurons we generated a Split-GAL4 stock: R22E09_AD inserted in attp40 (chromosome 2L) and R12C03_DBD

in attp2 (3L) (JRC-SS00888). To selectively target griddle-2 neurons we generated a Split-GAL4 stock R55C05_AD inserted in attp40 (chromosome 2L) and R32D04_DBD

in attp2 (3L) (JRC-SS00918). To selectively target ladder-d neurons we generated a Split-GAL4 stock R78F07_AD inserted in attp40 (chromosome 2L) and R28E11_DBD in attp2 (3L) (JRC-SS00863). To selectively target drunken-1 and drunken-2 neurons we generated a Split-GAL4 stock R23A05_AD inserted in attp40 (chromosome 2L) and R48D11_DBD in attp2 (3L) (JRC-SS00674). The line for selective targeting of basin-4 was generated as described previously (Ohyama et al., 2015). AD and DBD combinations were assembled in a $w^{1118}$ background.

These GAL4 combinations (from the Rubin GAL4 collection) were chosen based on stochastic labeling of single cells (using a FLP-based approach) that revealed that above GAL4 combination both contained the cell(s) of interest, namely basin-2, basin-1, drunken-1 and 2, griddle-2, ladder-d. The 'FLP-out' approach (Struhl and Basler, 1993) for stochastic single-cell is described in detail elsewhere (Nern et al., 2015). In brief, heat-shock induced expression of FLP recombinase was used to excise FRT-flanked interruption cassettes from UAS reporter constructs carrying HA, V5, and Flag epitope tags, and stained with epitope-tag specific antibodies. This labeled a subset of the cells in the expression pattern with a stochastic combination of the three labels.

To perform electrophysiology experiments we made the following stocks:

- –20B01-LexAp65 (JK22c); 20xUAS-CsChrimson-mCherry-trafficked in su(Hw)attP1, 13xLexAop2-IVS-GCaMP6s-p10 50.641 in VK5 (Chen et al., 2013; Klapoetke et al., 2014).
- -R72F11-p65ADZp in attP40; R38H09-ZpGdbd in attP2 (JRC-SS00739), UAS-GCamp6f 15.693 in VK0005 (Chen et al., 2013; Klapoetke et al., 2014).
- - w;20B01-LexA/CyO;13Lexop2 myr:: TDTomato/MKRS (Pfeiffer et al., 2012).

20xUAS-CsChrimson-mCherry-trafficked in su(Hw)attP1 is gift from V. Jayaraman, unpublished stock (Chen et al., 2013; Klapoetke et al., 2014), 13xLexAop2-IVS-GCaMP6s-p10 50.641 in VK000005, is gift from the GENIE project (JANELIA, HHMI), unpublished stock (Chen et al., 2013). LexAop2-myr::TDTomato-p10 (attp40), a gift from D. Mellert (Ohyama et al., 2015) is an myr::TDtomato fragment with AcNPV p10 (Pfeiffer et al., 2012). pGP-20XUAS-GCaMP6f-p10.92.693 in VK00005 is a gift from the GENIE project.

## METHOD DETAILS

### Behavioral Apparatus

The apparatus was described previously (Ohyama et al., 2013). Briefly, the apparatus comprises a video camera (DALSA Falcon 4M30 camera) for monitoring larvae, a ring light illuminator (Cree C503B-RCS-CW0Z0AA1 at 624 nm in the red), a computer (see Ohyama et al., 2013 for details); available upon request are the bill of materials, schematic diagrams and PCB CAM files for the assembly of the apparatus) and a hardware modules for controlling air-puff, controlled through multi worm tracker (MWT) software (http://sourceforge.net/projects/mwt) (Swierczek et al., 2011), as described in Ohyama et al. (2013). Air-puff is delivered as described previously (Ohyama et al., 2013). Briefly it is applied to a 25625 cm2 arena at a pressure of 1.1 MPa through a 3D-printed flare nozzle placed above the arena (with a 16 cm 6 0.17 cm opening) connected through a tubing system to plant supplied compressed air (0.5 MPa converted to a maximum of 1.4 MPa using a Maxpro Technologies DLA 5-1 air amplifier, standard quality for medical air with dewpoint of 210uC at 90 psig; relative humidity at 25uC and 32uC, ca. 1.2% and 0.9%, respectively). The strength of the airflow is controlled through a regulator downstream from the air amplifier and turned on and off with a solenoid valve (Parker Skinner 71215SN2GN00). Air-flow rates at 9 different positions in the arena were measure with a hot-wire anemometer to ensure even coverage of the arena (Extech Model 407119A and Accusense model UAS1000 by DegreeC). The air-current relay is triggered through TTL pulses delivered by a Measurement Computing PCI-CTR05 5-channel, counter/timer board at the direction of the MWT. The onset and durations of the stimulus is also controlled through the MWT.

### Behavioral Experiments

Embryos were collected for 8–16 hr at 25°C with 65% humidity. Larvae were raised at 25°C with normal cornmeal food. Foraging 3 instar larvae were used (larvae reared 72-84 hr or for 3 days at 25°C). Larvae with all optogenetic experiments were raised on food supplemented with all-trans retinal.

Before experiments, larvae were separated from food using 10% sucrose, scooped with a paint brush into a sieve and washed with water (as described previously). This is because sucrose is denser than water, and larvae quickly float up in sucrose making scooping them out from food a lot faster and easier. This method is especially useful for experiments with large number of animals. We have controlled for the effect and have seen no difference in the behavior between larvae scooped with sucrose and larvae scooped directly from the food plate with a forceps.

The larvae were dried and spread on the agar starting from the center of the arena. The substrate for behavioral experiments was a 3% Bacto agar gel in a 25625 cm2 square plastic dishes. Larvae were washed with water at room temperature, the dishes were kept at room temperature and the temperature on the rig inside the enclosure was set to 25°C. The humidity in the room is monitored and held at 58%, with humidifiers (Humidifirst Mist Pac-5 Ultrasonic Humidifier).

We tested approximately 50–100 larvae at once in the behavioral assays. The temperature of the entire rig was kept at 25°C. In the assay the larvae were left to crawl freely on an agar plate for 44 s prior the stimulus delivery. The air-puff was delivered at the 45$^{th}$ second and applied for 38 s. After a period of recovery of about 20 s when 10 air-puff pulses, 2 s each, were delivered (with a 8 s separation interval).

In the assay with exogenous neuronal activation CsChrimson was activated using a 617-nm wavelength LED, with an irradiance of 296-425 $\mu$W/ cm$^2$, as measured from the location of the preparation. The arena was illuminated from below through clear agar. The larvae crawled freely for 30 s prior to light delivery by switching the LED on for 15 s.

The MWT software64 (http://sourceforge.net/projects/mwt) was used to record all behavioral responses.

### Mechanical and Optogenetic Stimulation for Electrophysiology Recordings

Mechanical stimulation was generated by arbitrary waveform generator (33220A, Agilent Technologies) and amplified by a stereo power amplifier (PCA3, Pyle Pro). The stimulation signal was delivered to a quick-mount extension actuator (Piezo Systems, Inc.), which was embedded in the sylgard-coated recording chamber. The stimulation was set at 1000Hz, with the intensity of 40 V and duration of 10-50 ms.

CsChrimson was activated using a 617-nm wavelength LED, with irradiance of 320 $\mu$W/ cm2, as measured from the location of the preparation. The LEDs was on for 10-50 ms.

We note there is a drastic difference in context between the optogenetic activation experiments in the dissected preparation and the freely behaving animals. In the dissected preparation, the body wall and the light-sensing organs in the front are damaged, and the animal is not moving. Feedback from proprioceptive neurons and from copies of motor commands is absent, or abnormal, high levels of nociceptive stimulation are present (due to injury of the body wall), and the light stimulus used for optogenetic activation is likely not sensed. The effective light intensity may be much higher, because the light does not need to penetrate through the cuticle before it reaches the CNS (even though the actual light intensities used were very similar, 320 $\mu$W/cm$^2$ in electrophysiology, and 296-425 $\mu$W/cm$^2$ in behavior). In the freely behaving animals, both proprioceptive feedback and copies of motor commands are present and nociceptive stimulation is absent. Furthermore, larvae do see and react to the red light (617 nm), at intensities used for optogenetic stimulation, by increasing the probability of bending. A large difference in context between the dissected preparation and the freely behaving animal is also present for the mechanosensory stimulation experiments. The absolute magnitudes of mechanical stimulation (g-force 1.12 m/s$^2$ in electrophysiology and behavior) and LED light intensity (ca. 300 - 400 $\mu$W/cm$^2$) that evoke reliable

behavioral responses and electrophysiological responses are similar. However, it is difficult to compare the effective magnitudes of stimulation in the electrophysiological preparations and freely behaving animals as in the former case the animals is dissected and its body wall is stretched and pinned (which could affect the responses of the mechanosensory neurons) and immersed in a physiological solution, whereas in the second case the animal is intact and the stimulus is delivered through air and from above.

### Whole-Cell Patch-Clamp Recordings from Basin Neurons in Ventral Nerve Cord

The experiments were performed on third instar larvae at feeding stage. Fillet preparations with ventral nerve cord (VNC) attached were dissected in Baines external solution, which contained (mM): 135 NaCl, 5 KCl, 2 CaCl2.2H2O, 4 MgCl2.6H2O, 5 2-[(2-Hydroxy-1,1-bis(hydroxymethyl)ethyl)amino] ethanesulfonic acid, N-[Tris(hydroxymethyl) methyl] −2-aminoethanesulfonic acid, and 36 sucrose. The pH was adjusted to 7.15 with NaOH, and osmolarity was 310-320.

The larvae were cut all the way along the dorsal surface, and the fillet was pinned down at 4 corners onto the sylgard-coated recording chamber using fine wire (0.001 tungsten 99.95% wire; California Fine Wire Company). The guts were removed carefully to avoid nerve damage. To minimize VNC movement during the recordings, a transverse cut was made on the anterior cuticle and body wall retracted toward posterior, so that a tiny piece of parafilm could be placed underneath of VNC. The nerves connecting the cuticle and VNC were "glued" to parafilm using petroleum jelly. The preparation was viewed with a 60 × /1 N.A. water-immersion objective equipped with Olympus microscopy (BX51WI; Olympus). GcAMP6 –labeled basin neurons were visualized with a 470-nm wavelength LED. A small section of the glial sheath above the targeted abdominal basin neurons was ruptured using protease (0.1% Protease XIV; Sigma-Aldrich). Recording electrodes were pulled from thick-wall glass pipet (O.D. 1.5mm, I.D. 0.86mm) using P-97 puller (Sutter Instruments) and fire-polished to resistances of 10–15 MΩ. The Baines intracellular solutions contained (mM): 140 potassium gluconate, 5 KCl, 2 MgCl2.6H2O, 2 EGTA, 20 HEPES. The pH was adjusted to 7.4 with KOH, and the osmolarity was 280. The intracellular solution contained 0.5% Neurobiotin for the further post hoc morphological identification of recorded neurons. The data were acquired and processed using Digidata 1440A, Multiclamp 700B, and Clampex 10.4 software (Molecular Devices). The recording was sampled at 20 kHz and filtered at 6 kHz under current-clamp mode, and 10 KHz and 2 KHz under voltage-clamp mode. The recordings will not be processed for further analysis if the resting membrane potential at cell body became > −45 mV before correcting liquid junction potential (15mV) corrections.

### Basin Neuron Identification

After the electrophysiology recording, the preparation containing VNC and brain was fixed in 4% paraformaldehyde in 0.1 M phosphate buffer saline (PBS) overnight in refrigerator, and then transferred to PBS until staining. After rinsing in PBS, the CNS preparations were placed in Streptavidin Alexa Fluor 647 (1:200) in PBS-T (overnight, room temperature). After rinsing, the preparations were dehydrated and mounted with DPX. The confocal images were captured with Zeiss 710 confocal laser microscope. Alexa Fluor 647 was excited with a light of 633 nm wavelength, and mcherry-tagged CsChrimson neurons were excited with a light of 567 nm.

### Spike Detection in Electrophysiological Recordings of Basin Neurons

Many insect neurons are non-spiking and influence downstream partners only through graded potentials. Some insect interneurons use, both action potentials and graded potentials, for signal transmission (Burrows and Siegler, 1976; Hengstenberg, 1977; Milde, 1981; Pearson, 1976). It is likely that Basins use both the graded potentials and the APs, for signal transmission and for influencing behavioral output.

Like most insect neurons, Basin cell bodies are closer to the dendritic tree, than to the axon terminal, but they are separated from both by a long primary neurite. The synaptic potentials generated at the dendritic tree therefore bypass the soma on the way to the main spike initiation zone (SIZ), likely located at the start of the axon, just after bifurcation of the primary neurite into a dendritic and an axonal branch (Gouwens and Wilson, 2009).

The SIZ is much closer to the axon terminals (ca. 24 μm in 3$^{rd}$ instar larva), than to the cell body (ca. 60 μm away in 3$^{rd}$ instar larva). The depolarizations at the axon terminal are likely much larger than the ones we observe at the cell body. Thus, graded potentials observed in Basin neuron cell bodies are likely to propagate all the way to the axon terminal and influence their downstream partners and behavior, and not only APs.

Furthermore, because the cell bodies (where the patch-clamp recordings are performed) are very far from the SIZ, it is likely that we do not detect many APs evoked by mechanosensory or optogenetic stimuli, because they are distorted and reduced in amplitude (due to distance). When such APs occur on top of large fluctuating depolarizations it is difficult to detect them. In the current injection experiments APs are much easier to detect, because they are not distorted by riding on large EPSPs.

### GABA Histochemistry Labeling

To determine the neurotransmitter identification in the interneurons, GABA immune-labeling was performed from the JRC-SS00888 (handle-b), JRC-SS00918 (griddle-2), JRC_SS00674 (drunken-1 and drunken-2), JRC-SS00863 (ladder-d) crossed to pJFRC12-10XUAS-IVS-myr::GFP. The VNC was dissected out from 3rd instar larvae, and fixed with 4% PFA for 30 min. After rinsing in PBS, the CNS preparations were incubated in the rabbit anti-GABA (1:500, Sigma) and chick anti-GFP (1:1000, abcam) in PBS-T, followed by Alexa Fluor 488 goat anti-chick IgG and Alexa Fluor 647 goat anti-rabbit IgG. After rinsing, the preparations were

dehydrated and mounted with DPX. The confocal images were captured with Zeiss 710 confocal laser microscope. Alexa Fluor 488 was excited with a light of 488 nm, while Alexa Fluor 647 was excited with a light of 633 nm wavelength.

## EM Reconstruction and Wiring Diagrams

EM reconstruction followed the procedures described in (Schneider-Mizell et al., 2016) and (Ohyama et al., 2015). Briefly, we performed manual annotation of serial EM sections in a web-based tool CATMAID (http://www.catmaid.org) (Saalfeld et al., 2009), which allowed for fast reconstruction of neuronal skeletons, which express the anatomy and topology of neural arbors but lack volumetric information, and connectivity. To ensure accuracy, reconstructions were followed by a later comprehensive review (Schneider-Mizell et al., 2016). To focus on those neurons involved in segmental microcircuits connecting chordotonal sensory terminals and Basin dendrites, we looked at the 1.5 segment first instar volume in which all arbors downstream of chordotonal axons were reconstructed (Ohyama et al., 2015). This identified the iLNa interneurons described here and a subset of Ladder neurons, but the precise identity of which Ladders could not be determined because key identifying features were located outside of the smaller imaged volume. We continued this work in a second volume spanning the entire first instar CNS (Ohyama et al., 2015) by performing targeted reconstruction of all Ladders, Drunken-1, Griddle-1, and Griddle-2 in segment a1 and any appropriate nearby segments. Manual reconstructions of neuronal anatomy and connectivity were performed and reviewed by author CMSM with significant contributions from Ingrid Andrade, Javier Valdes Aleman, Laura Herren, Waleed Osman, and incidental contributions from fourteen other contributors working in the same dataset. It is possible that additional interneurons between chordotonal and Basin cells may exist if their structure was not uniquely identifiable in the previous volume. Existing reconstructions of chordotonal axon terminals, Basin cells in segments, fbLN-Ha, and fbLN-Hb from segment a1 were taken from prior reconstructions (Ohyama et al., 2015). Small differences between anatomy and connectivity of previously reconstructed neurons are due to correction of errors that were noticed during subsequent reconstruction, typically in the form of omitted twigs, small branches hosting few synapses that have little impact on the network topology (Schneider-Mizell et al., 2016).

For wiring diagram descriptions at the cell type level, we summed the number synapses in a given connection between cell types if that connection was reliably found with 3 or more synapses on both left and right sides of the animal. Individual neuron connectivity can be found in the Supplementary neuronal adjacency matrix. Connectivity was analyzed and visualized with custom Matlab (The Mathworks, Inc) scripts.

## Model

We built a rate model with units connected as per EM reconstructions and behavior output taken from silencing and activation experiments. For simplicity, each neuron category (mechano-ch, iLNa, iLNb, fbLN-Ha and fLN-Hb) was reduced to a single node and connections with small differences in synaptic count were made equal to reduce parameter choices. We described the system with a rate vector $\boldsymbol{r} \geq 0$, each element of which corresponds to a category of neurons (1: Mechano-ch, 2: Basin-1, 3: Basin-2, 4: iLNb, 5: iLNa, 6: fbLN-Ha, 7: fbLN-Hb). Activity followed the equation:

$$\tau_i \frac{dr_i}{dt} = -V_{0,i} - r_i + s_i + (r^{max} - r_i)\sum_j A_{ij}^{ex} r_j - \sum_j A_{ij}^{in} r_j$$

where $V_0$ sets the threshold for activation, $s_i$ is the stimulus input, $r^{max}$ sets the maximum rate, and $A_{ij}^{ex}$ and $A_{ij}^{in}$ are the excitatory and inhibitory connection strengths from neuron $j$ to neuron $i$, respectively. For the sensory element ($i = 1$ for clarity), $\tau_1 = 1$, $V_{0,1} = 0$ and $s_1 = 0$ before stimulus and $s_1 = 2$ during. The stimulus period lasted 450 time units, sufficient time to achieve equilibrium for parameters tested. To avoid introducing intrinsic timing differences arising from anything other than network topology, for all elements $i > 1$, $\tau_i = 35$, $V_{0,1} = 20$, and $s_1 = 0$ for all time. For all elements, $r^{max} = 20$. The connectivity matrices were:

$$A^{ex} = \begin{bmatrix} 0 & 0 & 0 & 0 & 0 & 0 & 0 \\ 1.5 & 0 & 0 & 0 & 0 & 0 & 0 \\ 0.75 & 0 & 0 & 0 & 0 & 0 & 0 \\ w_{iLNb} & 0 & 0 & 0 & 0 & 0 & 0 \\ w_{iLNa} & 0 & 0 & 0 & 0 & 0 & 0 \\ 0 & 0.2 & 0.2 & 0 & 0 & 0 & 0 \\ 0.4 & 0 & 0.5 & 0 & 0 & 0 & 0 \end{bmatrix}$$

$$A^{in} = \begin{bmatrix} 0 & 0 & 0 & 0 & 0 & 0 & 0 \\ 0 & 0 & 0 & 1.7648 & 1.3841 & 0 & 0 \\ 0 & 0 & 0 & 1 & 5.9167 & 0 & 0 \\ 0 & 0 & 0 & 0 & 3.3744 & 1.6659 & 2.191 \\ 0 & 0 & 0 & 2.7133 & 0 & 1.1010 & 3.3031 \\ 0 & 0 & 0 & 1.8411 & 1.1158 & 0 & 0 \\ 0 & 0 & 0 & 1.7331 & 2.2145 & 0 & 0 \end{bmatrix}$$

Values for the inhibitory connectivity were drawn directly from the number of synapses observed in the reconstructions between cell categories, normalized to the iLNb-to-Basin-2 edge, in order to approximate connection strength. Values for the excitatory connectivity were approximated from synaptic counts, with the overall amplitudes chosen to generate diverse dynamics. The sensory input into iLNa and iLNb, $w_{iLNa}$ and $w_{iLNb}$ was chosen between 0.5–1.5 for iLNa and 1.5–2.5 for iLNb to represent differences in sensory activation of the two interneuronal classes by differential activation of the pattern of sensory inputs. Dynamics were solved by numerical integration using the *ode45* function in Matlab 2014b (Mathworks, Inc) with the 'nonnegative' option. Neurons were silenced in the model by setting all input and output weights to 0.

Following the computation of dynamics, the hunch/turn behavior was determined from the Basin-1 and Basin-2 activity rates. Inspired by the genetic silencing experiments, we set a hunch reaction to occur when Basin-1 was more strongly active than Basin-2, a bend reaction when Basin-2 is near or more active than Basin-1, and no reaction when neither are strong. For concreteness, we based the behavior function on $\hat{r}_2 = r_2/r_2^*$ (Basin-1 activity) and on $\hat{r}_3 = r_3/r_3^*$ (Basin-2 activity), where $r_i^*$ is the maximum values of $r_i$ for dynamics when $w_{iLNa} = 1$ and $w_{iLNb} = 2$, the center of the landscape we describe.

$$\text{No response} : \hat{r}_2 \leq 0.5 \; AND \; \hat{r}_3 \leq 0.5$$

$$\text{Hunch} : \frac{\hat{r}_3}{\hat{r}_2} < 0.8 \; AND \;\; \hat{r}_2, \hat{r}_3 > 0.5$$

$$\text{Turn} : \frac{\hat{r}_3}{\hat{r}_2} \geq 0.8 \; AND \;\; \hat{r}_2, \hat{r}_3 > 0.5$$

Values were chosen to highlight a full range of states. Note that because of Basin-1 receives stronger input than Basin-2, even without inhibition Basin-2 will respond slightly slower than Basin-1. We did not count states that lasted less than twice the duration between "no reaction" to "bend" in the case of excitation without any inhibition, this was approximately 16 time units.

## QUANTIFICATION AND STATISTICAL ANALYSIS

### Behavior Quantification

Larvae were tracked in real-time using the MWT software (Swierczek et al., 2011). We rejected objects that were tracked for less than 5 s or moved less than one body length of the larva. For each larva MWT returns a contour, spine and center of mass as a function of time. From the MWT tracking data we computed the key parameters of larval motion, using specific choreography (part of the MWT software package) variables (Ohyama et al., 2013). From the tracking data, we detected and quantified hunching and bending events and peristaltic crawling strides as described in (Ohyama et al., 2013), using the LARA software package (http://sourceforge.net/projects/salam-hhmi). For optogenetic experiments, because a roll can be evoked by optogenetically activating basin-type neurons (Ohyama et al., 2015), a behavior classification that allows better discriminations between roll and hunch actions than the LARA behavior classification method (Ohyama et al., 2013) was used. Behavior classification is performed using supervised learning based on human tagging of larval video. It is performed on a very limited set of features exhibiting low variance under the mechanical deformations induce by the larval dynamics. It consists on a 3-layer procedure. The first layer relies on Random Forest (Breiman, 2001) to identify if one of the listed behavior is being performed and output a Boolean variable. The second layer collects all states and check for inconsistencies (e.g., a larva crawling and head-casting at the same time). The third layer uses Hidden Markov model to perform the final behavior assessment (Bishop, 2006).

To calculate the fraction animals hunching and bending in response to air-current in the tested population of larvae, we calculated the number of animals that hunched or bent at least once during the sampling time-interval (20 s time interval following stimulation) as well as during 20 s time window preceding the stimulation. We used the number of larvae that hunched and bent during the pre-stimulus detected events as an estimate of any spontaneous behaviors occurring also during the response to air-current. The number of detected hunches in a pre-stimulus time window was very small as hunch is a type of startle response happening mostly in response to a stimulus (Ohyama et al., 2013). Bends, on the other hand occur frequently prior to stimulus delivery as larvae perform the search behavior during foraging. To calculate the fraction animals hunching and bending upon optogenetic activation of key neurons in the tested population of larvae, we calculated the number of animals that hunched or bent at least once during the sampling time-interval (5 s) after the onset of red light.

### Transition Probabilities

To calculate transition probabilities, we computed the total number of post-stimulus transitions from each behavior (crawl, hunch, or bend) to one of the other two across all animals in the population and normalized this by the number of all transitions from the same behavior. Transitions were considered genuine post-stimulus events if they started 0.05 s after air-puff onset and lasted at least 0.02 s. The transition probabilities starting from a given behavior for control and experimental populations were statistically compared by the Fisher exact test.

## Statistical Analysis

All data, except those from animals that were not tracked for more than 5 s (see behavioral quantification) were included in the quantitative analysis. All statistical tests and significance levels for data comparisons are specified in the results section of the text or figure captions and are two-sided.

We performed a Fisher exact test to compare transitions probabilities in experimental lines and their respective controls.

We performed paired t test to compare electrophysiological recordings between different conditions.

In order to detect the effects of silencing of individual neuron types (chordotonals, basin-1, basin-2, griddle-2, handle-b, basin-4) on hunching and bending in response to air-puff, we computed an estimator intended to detect the emergence of behaviors at the population scale. We computed the ratio of larvae bending and hunching at least one time in the 20 s sampling time window before, respectively $p_B^b$ and $p_B^h$, and after stimulus, respectively $p_A^b$ and $p_A^h$. The ratios were defined as $p_k^i = (N_k^i / N_k^{all})$ with $i \in \{b,h\}, k \in \{A,B\}$ and $N_k^{all}$ the total number of larva during the 20 s time window. In order to quantify the effect of the stimulus we defined $\chi^i(p) = p_A^i - p_B^i$ as the difference in the ratio after and before the stimulus with $i \in \{b,h\}$. Note that results are not time window duration dependent for duration superiors to 5 s. In order to compare tests line our estimator was defined as

$$\Theta^i(p,q) = \chi^i(p) - \chi^i(q),$$

with p and q the ratios of the lines and the control respectively. $\Theta^i(p,q)$ takes value in [-1,1]. $\Theta^i(p,q)$ is null if there are no differences between the line tested and the control. Positive or negative values indicate an effect of neuron silencing when compared to the control. Statistical testing for significance was performed against a null hypothesis of $\Theta^i(p,q) = 0$ with $p_k^i = q_k^i$. p-values were evaluated using numerical simulations where $\{p_k^i, q_k^i\}$ were generated from hypergeometric distributions.

The pseudo code to generate the p-value reads:

- Repeat $\boldsymbol{N_{sim}} = 5.10^5$ times
- $\boldsymbol{N_{out}} = 0$
- $\boldsymbol{n_B^i(p)} \sim \text{Hyper}(\boldsymbol{N_B^{all}(p)} + \boldsymbol{N_B^{all}(q)}, \boldsymbol{N_B^i(p)} + \boldsymbol{N_B^i(q)}, \boldsymbol{N_B^i(p)})$
- $\boldsymbol{n_B^i(q)} = \boldsymbol{N_B^{all}(p)} + \boldsymbol{N_B^{all}(q)} - \boldsymbol{n_B^i(p)}$
- $\boldsymbol{n_A^i(p)} \sim \text{Hyper}(\boldsymbol{N_A^{all}(p)} + \boldsymbol{N_A^{all}(q)}, \boldsymbol{N_A^i(p)} + \boldsymbol{N_A^i(q)}, \boldsymbol{N_A^i(p)})$
- $\boldsymbol{n_A^i(q)} = \boldsymbol{N_A^{all}(p)} + \boldsymbol{N_A^{all}(q)} - \boldsymbol{n_A^i(p)}$
- evaluate $\chi^i(\boldsymbol{p}) = \frac{\boldsymbol{n_A^i(p)}}{\boldsymbol{N_A^{all}(p)}} - \frac{\boldsymbol{n_B^i(p)}}{\boldsymbol{N_B^{all}(p)}}$, $\chi^i(\boldsymbol{q}) = \frac{\boldsymbol{n_A^i(q)}}{\boldsymbol{N_A^{all}(q)}} - \frac{\boldsymbol{n_B^i(q)}}{\boldsymbol{N_B^{all}(q)}}$ and $\Theta^i(\boldsymbol{p},\boldsymbol{q}) = \chi^i(\boldsymbol{p}) - \chi^i(\boldsymbol{q})$
- if $\Theta^i(\boldsymbol{p},\boldsymbol{q}) \geq \Theta^i_{exp}(\boldsymbol{p},\boldsymbol{q})$, $\boldsymbol{N_{out}} = \boldsymbol{N_{out}} + \boldsymbol{1}$
- end repeat
- evaluate $\boldsymbol{p} = \frac{\boldsymbol{N_{out}}}{\boldsymbol{N_{sim}}}$

With $\sim$ the symbol for drawing from a distribution and $\text{Hyper}(N_1, N_2, N_3)$ the hypergeometric distribution with $N_1$ the total number of elements, $N_2$ the number of elements with a specific characteristic (here for example bending) and $N_3$ the number of elements drawn.

Note that this estimator, $\Theta^i(p,q)$, has the advantage of being able to detect the non-synchronous emergence of a behavior at a population scale. For example, bending can either emerge as an immediate response to the puff or as the second response after hunching. The statistics of start time of bending is thus widely distributed at the population scale. Time evolution of instantaneous ratio of larva performing bending would not exhibit a strong increase after stimuli because larvae are not all going to bend immediately after stimuli. $\Theta^i(p,q)$ by accumulating events during a time window allows efficient detection of a behavior even if it is widely distributed in time.

We also performed a chi-square test to compare proportions of larvae hunching and bending upon optogenetic stimulation in test and control larvae.